GRAVMAD: GROUNDED SPATIAL VALUE MAPS GUIDED ACTION DIFFUSION FOR GENERALIZED 3D MANIPULATION

Anonymous authors
Paper under double-blind review

ABSTRACT

Robots' ability to follow language instructions and execute diverse 3D manipulation tasks is vital in robot learning. Traditional imitation learning-based methods perform well on seen tasks but struggle with novel, unseen ones due to variability. Recent approaches leverage large foundation models to assist in understanding novel tasks, thereby mitigating this issue. However, these methods lack a task-specific learning process, which is essential for an accurate understanding of 3D environments, often leading to execution failures. In this paper, we introduce **GravMAD**, a sub-goal-driven, language-conditioned action diffusion framework that combines the strengths of imitation learning and foundation models. Our approach breaks tasks into sub-goals based on language instructions, allowing auxiliary guidance during both training and inference. During training, we introduce **Sub-goal Keypose Discovery** to identify key sub-goals from demonstrations. Inference differs from training, as there are no demonstrations available, so we use pre-trained foundation models to bridge the gap and identify sub-goals for the current task. In both phases, **GravMaps** are generated from sub-goals, providing GravMAD with more flexible 3D spatial guidance compared to fixed 3D positions. Empirical evaluations on RLBench show that GravMAD significantly outperforms state-of-the-art methods, with a 28.63% improvement on novel tasks and a 13.36% gain on tasks encountered during training. Evaluations on real-world robotic tasks further show that GravMAD can reason about real-world tasks, associate them with relevant visual information, and generalize to novel tasks. These results demonstrate GravMAD's strong multi-task learning and generalization in 3D manipulation. Video demonstrations are available at: `https://gravmad.github.io`.

1 INTRODUCTION

One of the ultimate goals of general-purpose robot manipulation learning is to enable robots to perform a wide range of tasks in real-world 3D environments based on natural language instructions (Hu et al., 2023a). To achieve this, robots must understand task language instructions and align them with the spatial properties of relevant objects in the scene. Additionally, robots must effectively generalize across different tasks and environments; otherwise, their practical application will be limited Zhou et al. (2023). For example, if a robot has learned the policy for the task *"Take the chicken off the grill"*, it should also be able to perform the task *"Put the chicken on the grill"*. Without this generalization ability, its utility will be greatly reduced. Recent research in robot learning for 3D manipulation tasks has focused on two mainstream approaches: imitation learning-based methods and pre-trained foundation model-based methods. Imitation learning-based methods learn end-to-end policies from expert demonstrations in attempt to address 3D manipulation tasks (Walke et al., 2023; Padalkar et al., 2024; Argall et al., 2009). By designing various learning frameworks, such as incorporating different 3D representations (Shridhar et al., 2023; Chen et al., 2023; Goyal et al., 2023), policy representations (Ze et al., 2024; Ke et al., 2024; Yan et al., 2024), and multi-stage architectures (Gervet et al., 2023; Goyal et al., 2024), imitation learning-based policies can map perceptual information and language instructions to actions that complete complex 3D manipulation tasks. However, these policies often overfit to specific tasks (Xie et al., 2024; Zhang et al., 2024), leading to significant

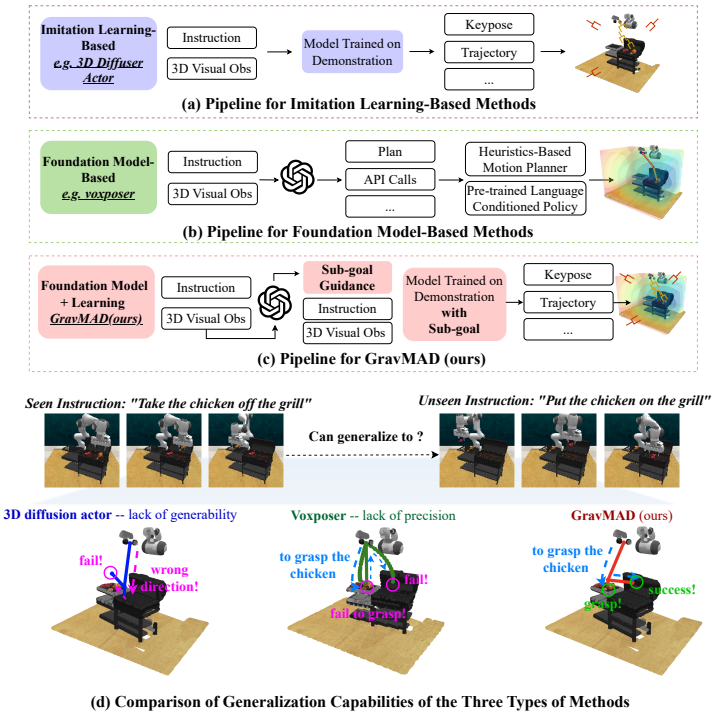

Figure 1: **Comparison of Pipelines.** (a) Imitation learning-based methods learn end-to-end policies that map language and 3D observations to actions for precise manipulation. (b) Foundation models-based methods use LLMs/VLMs to process inputs, generate plans, and execute actions with predefined primitives for task generalization. (c)(d) GravMAD combines both, using sub-goal guidance to leverage the language understanding of foundation models and the policy learning of imitation learning for precise and generalized manipulation.

performance degradation or even failure when applied to tasks that differ from those encountered during training (Brohan et al., 2023a; Zitkovich et al., 2023).

Another line of cutting-edge research seeks to leverage foundation models trained on internet-scale data (OpenAI, 2023; Yang et al., 2023b) to enhance policy generalization across a variety of tasks (Brohan et al., 2023b; Hu et al., 2023b; Huang et al., 2023). Unlike traditional imitation learning-based methods, approaches using pre-trained foundation models typically decouple perception, reasoning, and control during manipulation (Sharan et al., 2024). However, this decoupling often leads to a limited understanding of scenes and manipulation tasks (Huang et al., 2024), allowing robots to conceptually grasp tasks but failing to accurately complete tasks in 3D environments, resulting in failures. This underscores a key challenge: both imitation learning-based and foundation model-based approaches struggle to balance precision and generalization when adapting to novel 3D manipulation tasks. Such a challenge raises a crucial question: *Can the strengths of both approaches be combined to achieve precise yet generalized 3D manipulation?*

To this end, inspired by the approach of introducing task sub-goals to achieve efficient execution in robotic manipulation (Black et al., 2024; Kang et al., 2023; Xian et al., 2023; Ma et al., 2024), we propose discovering key sub-goals for 3D manipulation tasks as a bridge between foundation models and learned policies, leading to the development of **Gr**ounded Sp**a**tial **V**alue **M**aps-guided **A**ction **D**iffusion (**GravMAD**), a novel sub-goals-driven, language-conditioned action diffusion framework. Specifically, a new data distillation method called **Sub-goal Keypose Discovery** is introduced during the training phase. This method identifies the key sub-goals required for each sub-task stage from the demonstrations. In the inference phase, pre-trained foundation models are leveraged to interpret the robot's 3D visual observations and task language instructions, directly identifying task sub-goals. Once the task sub-goals are obtained, the voxel value maps introduced in Voxposer (Huang et al., 2023) are used to generate the corresponding **Gr**ounded Sp**a**tial **V**alue **Map**s (**GravMaps**). These maps reflect both the cost associated with each sub-goal and the ideal gripper openness. The closer to the sub-goal, the lower (cooler) the cost; the farther away, the higher (warmer) the cost, while also indicating the gripper's state within the sub-goal range. Thus, they serve as intuitive tools for

grounding language instructions into 3D robotic workspaces. Finally, the generated GravMaps are integrated with the policy diffusion architecture proposed in 3D diffuser actor (Ke et al., 2024), forming the GravMAD framework. This enables the robot to utilize 3D visual observations, task language instructions, and GravMaps guidance to denoise random noise into precise end-effector poses. As shown in Fig. 1, GravMAD effectively combines the precise manipulation capabilities of imitation learning-based methods with the reasoning and generalization abilities of foundation model-based approaches. We extensively evaluate GravMAD on RLBench (James et al., 2020a), a representative benchmark for instruction-following 3D manipulation tasks. The results show that GravMAD not only performs well on tasks encountered during training but also significantly outperforms state-of-the-art baseline methods in terms of generalization to novel tasks. Additionally, we validate these findings through 10 real-world robotic manipulation tasks.

In summary, our contributions are: **1)** We propose leveraging key sub-goals in 3D manipulation tasks to bridge the gap between foundation models and learned policies. In the training phase, we introduce a data distillation method, **Sub-goal Keypose Discovery**, to identify task sub-goals. In the inference phase, foundation models are used for this purpose. **2)** We generate **GravMaps** from these sub-goals, translating task language instructions into 3D spatial sub-goals and reflecting spatial relationships in the environment. **3)** We propose a new action diffusion framework, **GravMAD**, guided by GravMaps. It is sub-goal-driven and language-conditioned, combining the precision of imitation learning with the generalization capabilities of foundation models. **4)** The simulation experiments are conducted on 20 tasks in RLBench, comprising two types: 12 base tasks directly selected from RLBench, and 8 novel tasks created by modifying scene configurations or task instructions. GravMAD achieves at least **13.36%** higher success rates than state-of-the-art baselines on the 12 base tasks encountered during training, and surpasses them by **28.63%** on the 8 novel tasks, highlighting its strong generalization capabilities. Experiments on 10 real-world robotic tasks further validate GravMAD's effectiveness.

2 Related Works

Learning 3D Manipulation Policies from Demonstrations. Recent works have employed various perception methods to learn 3D manipulation policies from demonstrations to tackle the complexity of reasoning in 3D space. These methods include using 2D images (Brohan et al., 2023a; Zitkovich et al., 2023; Jang et al., 2022), voxels (Shridhar et al., 2023; James et al., 2022), point clouds (Chen et al., 2023; Yuan et al., 2023), multi-view virtual images (Goyal et al., 2023; 2024), and feature fields (Gervet et al., 2023). To support policy learning, some studies (Ke et al., 2024; Xian et al., 2023; Yan et al., 2024; Ze et al., 2024) have integrated 3D scene representations with diffusion models (Ho et al., 2020). These approaches attempt to handle the multi-modality of actions, in contrast to behavior cloning methods that train deterministic policies. By leveraging 3D representation learning, these policies can accurately complete tasks by accounting for the spatial properties of objects, such as orientation and position. This is especially effective for tasks that closely resemble those encountered during training Ze et al. (2023). However, these policies often lack the language understanding and generalization abilities of foundation models. Our method builds upon the diffusion architecture (Ke et al., 2024), enhancing its ability to utilize demonstration data through imitation learning, while integrating foundation models to improve generalization, combining the strengths of both approaches.

Foundation Models for 3D Manipulation. Recent foundation models trained on internet-scale data have shown strong zero-shot and few-shot generalization, offering new opportunities for complex 3D manipulation tasks (Hu et al., 2023a; Zhou et al., 2023). While some approaches fine-tune vision-language models with embodied data (Driess et al., 2023; Li et al., 2024), this increases computational costs due to the large data requirements. Alternatively, foundational vision models can generate visual representations for 3D manipulation tasks (Zhang et al., 2024; 2023), but they often lack the reasoning capabilities needed for complex tasks. To address these challenges, some studies leverages large language models (LLMs) as high-level planners (Brohan et al., 2023b; Hu et al., 2023b; Huang et al., 2022), generating language-based plans executed by lower-level policies. Others utilize LLMs' code-writing abilities to control robots via API calls or to create value maps for planning robot trajectories (Liang et al., 2023; Huang et al., 2023). However, these methods often sacrifice precision due to a rough understanding of complex 3D scenes. Recent works have combined the reasoning capabilities of foundation models with fine-grained control in 3D manipulation to overcome this limitation (Huang et al., 2024; Sharan et al., 2024). For example, Huang et al. (2024) uses pre-trained vision-language models (VLMs) to provide spatial constraints and a nonlinear solver

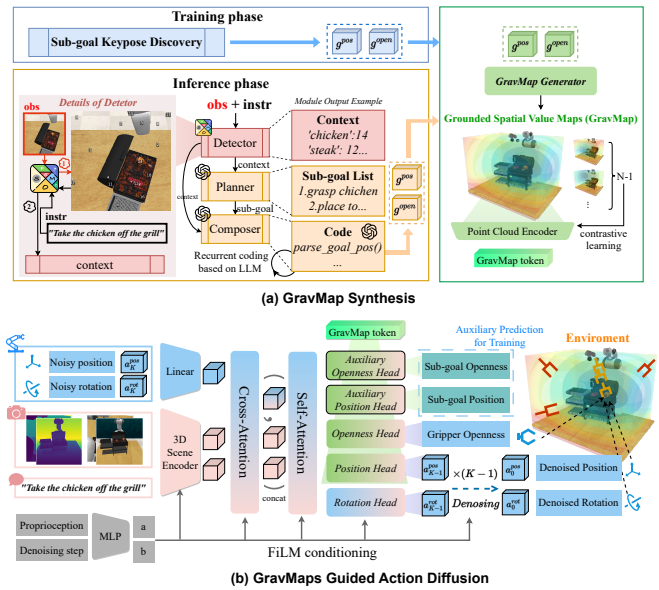

Figure 2: **GravMAD Overview. (a) GravMap Synthesis:** During training, we use Sub-goal Keypose Discovery to obtain sub-goals g^{pos} and g^{open}. During inference, the Detector, Planner, and Composer pipeline interprets visual observations and language instructions to derive g^{pos} and g^{open}, which are processed into a GravMap and encoded as a GravMap token. **(b) GravMaps Guided Action Diffusion:** The policy network perceives the scene and denoises noisy actions guided by the GravMap token. After K denoising steps, the clean actions are executed by the robot.

to generate precise grasp poses. Our method combines the learning power of diffusion architectures with the generalization of VLMs. VLMs generate spatial value maps that guide action diffusion, enabling precise control and multi-task generalization in 3D manipulation tasks.

3 METHOD

In this section, we introduce **GravMAD** (Grounded Spatial Value Maps Guided Action Diffusion), a multi-task, sub-goal-driven, language-conditioned diffusion framework for 3D manipulation, as shown in Fig. 2. We divide GravMAD's design into three parts: Section 3.1 defines the 3D manipulation problem, Section 3.2 explains the definition and generation of GravMaps, and Section 3.3 details how GravMaps guide action diffusion in 3D manipulation.

3.1 PROBLEM FORMULATION

We consider a problem setting where expert demonstrations consist of a robot trajectory $(o_1, a_1, o_2, a_2, \ldots)$ and a natural language instruction $\ell \in \mathcal{L}$ that describes the task goal. Each observation $o_t \in \mathcal{O}$ includes RGB-D images from one or more viewpoints. Each action $a_t \in \mathcal{A}$ contains the 3D position of the robot's end-effector $a^{\text{pos}} \in \mathbb{R}^3$, a 6D rotation $a^{\text{rot}} \in \mathbb{R}^6$, and a binary gripper state $a^{\text{open}} \in \{0, 1\}$. To address potential discontinuities from quaternion constraints and ensure smooth optimization, we utilize the 6D rotation representation (Ke et al., 2024). In this setting, we assume that a robotic task is composed of multiple sub-tasks, with each sub-task completed when the robot reaches a sub-goal $g_t \in \mathcal{G}$, which specifies the 3D position $g^{\text{pos}} \in \mathbb{R}^3$, the gripper openness $g^{\text{open}} \in \{0, 1\}$, and the 6D rotation $g^{\text{rot}} \in \mathbb{R}^6$. Based on this, we construct a new dataset $\mathcal{D} = \{\zeta_1, \zeta_2, \ldots\}$ from expert demonstrations. Each demonstration ζ consists of trajectories with sub-goals $\{(o_1, g_1, a_1), (o_2, g_2, a_2), \ldots\}$ and the corresponding language instruction ℓ. Our goal is to learn a policy $\pi : (\mathcal{O}, \mathcal{L}, \mathcal{G}) \mapsto \mathcal{A}$, which maps observations o_t, sub-goals g_t, and instructions ℓ to actions a_t. To facilitate sub-task segmentation and efficiently learn the policy, we frame the robot's 3D manipulation learning problem as a keypose prediction problem following prior works (James & Davison, 2022; James et al., 2022; Goyal et al., 2023; Shridhar et al., 2023). Our model progressively predicts the next keypose based on current observations and uses a sampling-based motion planner (Klemm et al., 2015) to plan the trajectory between two keyposes. In the existing keypose

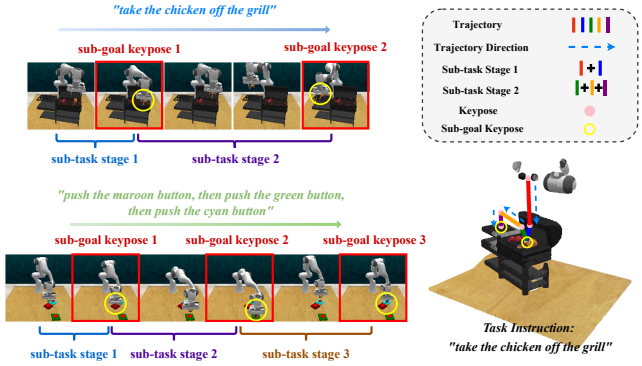

Figure 3: Visualization of sub-goal keyposes and sub-task stages. The left sub-figure shows image-based sub-goal keyposes and sub-task stages for *"take the chicken off the grill"* and *"push the __ button"* tasks. The right shows the sub-goal key poses and sub-task stages in the trajectory for the *"take the chicken off the grill"* task.

discovery method (James & Davison, 2022), a pose is identified as a keypose when the robot's joint velocities are near zero, and the gripper state remains unchanged. Our work filters the task's sub-goals based on these keyposes to facilitate sub-task segmentation and ensure efficient completion of the overall task.

3.2 GravMap: Grounded Spatial Value Maps

To tackle generalization challenges in 3D manipulation tasks, we introduce the spatial value maps (**GravMap**), an adaptation of the voxel value maps proposed by Huang et al., denoted as m. GravMaps are adaptively synthesized based on task variations, translating language instructions into 3D spatial sub-goals and reflecting the spatial relationships within the environment. This provides precise guidance for robotic action diffusion. Each GravMap m contains two voxel maps: (1) a spatial cost map m_c, with lower values near the sub-goal and higher costs further away, and (2) a gripper openness map m_o, indicating where the gripper should open or close. As shown in Fig. 2(a), GravMaps are generated differently for training and inference. In training, they are identified from expert demonstrations using the sub-goal keypose discovery method. During inference, pre-trained models generate them from language instructions and observed images.

GravMap Synthesis with Sub-goal keypose Discovery during Training. We define each sub-task stage in 3D manipulation as: (1) the process where the robotic end-effector transitions from not touching an object to making contact, or (2) the interaction between the end-effector or tool and a new object, where a series of operations are performed before disengaging. To efficiently segment these sub-task stages and find sub-goals, we build upon the existing keypose discovery method (James & Davison, 2022) and propose a novel data distillation method called **sub-goal keypose discovery**.

The sub-goal keypose discovery process iterates over each keypose $K_p^i \in \{K_p\}_1^{N_k}$, where N_k is the number of keyposes in a task. For each keypose, the corresponding observation-action pair $(o_{K_p^i}, a_{K_p^i})$ is passed to the function S_K, which outputs a Boolean value to determine whether the given keypose should be discovered as a sub-goal keypose. The decision is made based on whether the keypose satisfies the discovery constraint: $S_K((o_{K_p^i}, a_{K_p^i})) = \begin{cases} 1, & \text{if discovery constraints are met} \\ 0, & \text{otherwise} \end{cases}$. The function S_K can incorporate multiple constraints. In our paper, we define two constraints for S_K, depending on the type of manipulation task, as shown in Fig. 3: (1) For grasping tasks, such as *"take the chicken off the grill"*, sub-goal keyposes are discovered based on the following constraints: a change in the gripper's open/close state and a significant change in touch force. (2) For contact-based tasks, such as *"push the __ button"*, sub-goal keyposes are discovered solely based on significant changes in touch force. For more details on sub-goal keypose discovery, please refer to Appendix A.1.

After discovering the sub-goal keyposes, the sub-task stages can be quickly segmented, and the corresponding sub-goals can be identified. The end-effector position g^{pos} and gripper openness g^{open} at these sub-goals are then input to the *Gravmap generator* to generate the GravMaps m for training. The process of the GravMap generator is illustrated in Algorithm 1, adapted from Huang et al. (2023).

Algorithm 1: GravMap Generation Process

Input: End-effector position g^{pos}, gripper openness g^{open}, map size S_m, offset range β_o, radius β_r, downsample ratio β_d, number of sampled points N_p
Output: GravMap m
begin
// Initialize spatial cost map m_c and gripper map m_g with size S_m^3
Initialize m_c and m_g with shape $S_m \times S_m \times S_m$;
// Convert g^{pos} from world coordinates (x, y, z) to voxel coordinates (i, j, k)
Extract $(x, y, z) \leftarrow g^{\text{pos}}$; Convert (x, y, z) to voxel coordinates (i, j, k);
// Apply random offsets $\delta_i, \delta_j, \delta_k$ to (i, j, k) for data augmentation
Sample $\delta_i, \delta_j, \delta_k \sim \text{Uniform}(-\beta_o, \beta_o)$;
Update voxel coordinates: $(i', j', k') = (i + \delta_i, j + \delta_j, k + \delta_k)$;
// Set m_c at (i', j', k') to 0 and 1 elsewhere
Set $m_c(i', j', k') = 0$;
Set $m_c(u, v, w) = 1$ for all other voxels (u, v, w);
// Compute Euclidean distance from (i', j', k') for all (u, v, w)
For each voxel (u, v, w), compute $D(u, v, w) = \sqrt{(u - i')^2 + (v - j')^2 + (w - k')^2}$
Normalize $m_c(u, v, w) = \frac{D(u,v,w)}{\max D}$;
// Set m_g within radius β_r of (i', j', k')
Set $m_g(u, v, w) = g^{\text{open}}$ for voxels where $D(u, v, w) \leq \beta_r$;
Downsample m_c and m_g by β_d;
Select N_p points $\{v_p\}$ from the downsampled m_c using Farthest Point Sampling (FPS);
// Construct GravMap m using sampled points
Form $m = \{(v_p, m_c(v_p), m_g(v_p))\}_{p=1}^{N_p}$;
return m;

GravMap Synthesis with Foundation Model during Inference. During the inference phase, we use pre-trained foundation models to synthesize GravMaps. First, to enable the robot to tie the task-related words with their manifestation in the 3D environment, we introduce a Set-of-Mark (SoM) (Yang et al., 2023a)-based Detector. This Detector uses Semantic-SAM (Li et al., 2023) to perform semantic segmentation on the observed RGB images and assigns numerical tags to the segmented regions. Next, the Detector uses GPT-4o to select task-relevant objects and their corresponding tags from the labeled images as contextual information $\mathcal{C}$. Based on the task instructions ℓ and the context $\mathcal{C}$ provided by the Detector, we apply the LLM-based Planner proposed by Huang et al. to infer a series of text-based sub-goals. Then, an LLM-based Composer (Huang et al., 2023) recursively generates code to parse each sub-goal. During execution, the code uses the context $\mathcal{C}$ to obtain the end-effector positions g^{pos} and gripper openness states g^{open} corresponding to each sub-goal. Finally, g^{pos} and g^{open} are fed into the *GravMap generator* shown in Algorithm 1, skipping the data augmentation process to generate the GravMaps. Details of this process can be found in Appendix A.2.2.

We synthesize the GravMaps via sub-goal keypose discovery during training or foundation models during inference. GravMaps m are then downsampled using farthest point sampling (FPS) and encoded into token t_m with the DP3 (Ze et al., 2024) encoder, a lightweight MLP network.

3.3 GravMaps Guided Action Diffusion

After obtaining the GravMaps, they can be used to guide the action diffusion process, as shown in Fig. 2(b). Before the diffusion process begins, the robot should first perceive the 3D environment.

3D Scene Perception. Building on previous works (Gervet et al., 2023; Ke et al., 2024), we use a 3D scene encoder to transform language instructions and multi-view RGB-D images into scene tokens, enhancing the robot's 3D scene perception. RGB images are encoded using a pre-trained CLIP ResNet50 backbone (Radford et al., 2021) and a feature pyramid network. These features are lifted into 3D feature clouds using 3D positions derived from depth images and camera intrinsics. Simultaneously, the CLIP language encoder converts task instructions into language tokens. These

tokens interact with the 3D feature cloud to generate scene tokens (t_s), enabling the robot to capture 3D environmental information.

GravMaps Guided Action Diffusion. GravMAD builds upon the 3D trajectory diffusion architecture introduced by 3D Diffuser Actor (Ke et al., 2024) and further integrates GravMap tokens t_m to guide the action diffusion process. Specifically, GravMAD models policy learning as the reconstruction of the robot's end-effector pose using diffusion probabilistic models (DDPMs) (Ho et al., 2020). The end-effector pose is represented as $e = (a^{\text{pos}}, a^{\text{rot}})$. Starting with Gaussian noise $e_K = \left(a_K^{\text{pos}}, a_K^{\text{rot}}\right)$, the denoising networks $\epsilon_\theta^{\text{pos}}$ and $\epsilon_\theta^{\text{rot}}$ perform K iterative steps to progressively reconstruct the clean pose $e_0 = \left(a_0^{\text{pos}}, a_0^{\text{rot}}\right)$:

$$\begin{aligned} a_{k-1}^{\text{pos}} &= \alpha\left(a_k^{\text{pos}} - \gamma\epsilon_\theta^{\text{pos}}\left(e_k, k, p, t_s, t_m\right) + \mathcal{N}\left(0, \sigma^2 I\right)\right), \\ a_{k-1}^{\text{rot}} &= \alpha\left(a_k^{\text{rot}} - \gamma\epsilon_\theta^{\text{rot}}\left(e_k, k, p, t_s\right) + \mathcal{N}\left(0, \sigma^2 I\right)\right), \end{aligned} \tag{1}$$

where α, γ, and σ are functions of the iteration step k, determined by the noise schedule. $\mathcal{N}\left(0, \sigma^2 I\right)$ is Gaussian noise. Here, p represents proprioceptive information (a short action history). The denoising networks use 3D relative position attention layers (Gervet et al., 2023; Xian et al., 2023; Ke et al., 2024), with FiLM (Perez et al., 2018) conditioning applied to each layer based on proprioception p and denoising step k. As shown in Fig. 2(b), after passing through linear layers, a_K^{pos} and a_K^{rot} are concatenated and attend to the 3D scene tokens t_s via cross-attention. A self-attention layer then refines this representation to produce end-effector contextual features. These features are processed by five prediction heads: the *Position Head*, *Rotation Head*, *Openness Head*, *Auxiliary Openness Head*, and *Auxiliary Position Head*. In all but the rotation head, contextual features undergo cross-attention with GravMap tokens, followed by an MLP to predict the target values. See Appendix A.3 for details.

The first two prediction heads predict the noise added to the original pose using the $L1$ norm, with the losses defined as:

$$\begin{aligned} \mathcal{L}_{\text{pos}} &= \|\epsilon_k^{\text{pos}} - \epsilon_\theta^{\text{pos}}\left(e_k, k, p, t_s, t_m\right)\|, \\ \mathcal{L}_{\text{rot}} &= \|\epsilon_k^{\text{rot}} - \epsilon_\theta^{\text{rot}}\left(e_k, k, p, t_s\right)\|, \end{aligned} \tag{2}$$

where iteration k is randomly selected, and ϵ_k^{pos} and ϵ_k^{rot} are randomly sampled as the ground truth noise.

The third prediction head is used to predict the gripper's open/close state, and we use binary cross-entropy (BCE) loss for supervision:

$$\mathcal{L}_{\text{open}} = \text{BCE}\left(f_\theta^{\text{open}}\left(e_k, k, p, t_s, t_m\right), a^{\text{open}}\right) \tag{3}$$

The last two prediction heads enable GravMAD to better focus on the ideal end-effector pose at sub-goals, with the loss functions defined as follows:

$$\begin{aligned} \mathcal{L}_{\text{aux\_pos}} &= \|g^{\text{pos}} - f_\theta^{\text{aux\_pos}}\left(e_k, k, p, t_s, t_m\right))\|, \\ \mathcal{L}_{\text{aux\_open}} &= \text{BCE}\left(f_\theta^{\text{aux\_open}}(e_k, k, p, t_s, t_m), g^{\text{open}}\right), \end{aligned} \tag{4}$$

where f_θ represents the pose prediction network in GravMAD, while g^{pos} and g^{open} denote the ground truth sub-goal positions and gripper openness, respectively.

In addition to the losses related to robot actions mentioned above, a contrastive learning loss is applied to enhance feature representations from GravMaps. Positive pairs are features from the same GravMap, while negative pairs come from different GravMaps. In each forward pass, one GravMap is extracted from the dataset, and $N-1$ different GravMaps are randomly generated. The loss maximizes similarity between positive pairs and minimizes it between negative pairs:

$$\mathcal{L}_{\text{con}} = -\frac{1}{N}\sum_{i=1}^{N}\log\frac{\exp(f_{g_i}\cdot f_{g_i}^{+}/T)}{\sum_{j=1}^{N}\exp(f_{g_i}\cdot f_{g_j}/T)}, \tag{5}$$

where T is the temperature parameter, f_{g_i} represents the feature of the i-th sample, and $f_{g_i}^{+}$ represents the positive feature of the i-th sample.

At this stage, the training objective of GravMAD can be formulated by combining the losses from Eq.2, 3, 4, and 5 as follows:

$$\mathcal{L}_{\text{GravMAD}} = \mathcal{L}_{\text{open}} + \omega_1\cdot\mathcal{L}_{\text{pos}} + \omega_2\cdot\mathcal{L}_{\text{rot}} + \omega_3\cdot\mathcal{L}_{\text{aux\_pos}} + \mathcal{L}_{\text{aux\_open}} + \omega_4\cdot\mathcal{L}_{\text{con}}, \tag{6}$$

where $\omega_1, \omega_2, \omega_3, \omega_4$ are adjustable hyperparameters. For more detailed implementation of GravMap and GravMAD, please refer to Appendix A.

4 EXPERIMENTS

We aim to answer the following questions: **(i)** Can GravMAD achieve superior generalization in novel 3D manipulation tasks compared to SOTA models? (See Sec. 4.2) **(ii)** Is GravMAD's performance competitive on the 3D manipulation tasks encountered during training? (See Sec. 4.3) **(iii)** What key design elements contribute significantly to GravMAD's overall performance? (See Sec. 4.4)

4.1 ENVIRONMENTAL SETUP

To thoroughly investigate these questions, we conduct our experiments on a representative instruction-following 3D manipulation benchmark, RLBench (James et al., 2020b). Simulation experiments are conducted on two types of tasks to provide a comprehensive evaluation of GravMAD. **1) Base tasks.** To evaluate GravMAD's performance across 3D manipulation tasks encountered during training, we select 12 base tasks from RLBench's 100 language-conditioned tasks, each featuring 2 to 60 variations in instructions, such as handling objects of different colors or quantities. For each base task, we collect 20 demonstrations for training and evaluate the final checkpoints using 3 random seeds over 25 episodes. Detailed descriptions of these tasks are provided in Appendix B.1. **2) Novel tasks.** To further test GravMAD's generalization capabilities, we modify the scene configurations or task instructions of several base tasks to create 8 novel tasks across 3 novelty categories as illustrated in fig. 10. These modifications introduce significant challenges for the robot regarding instruction comprehension, environmental perception, and policy generalization, as described in Appendix B.2. For each novel task, we evaluate the final checkpoints trained on the 12 base tasks. We use 3 random seeds over 25 episodes for each novel task. For all tasks, we use a front-view 256×256 RGB-D camera and a Franka Panda robot with parallel grippers. Additionally, we further validate GravMAD on 10 real-world robotic tasks, with details provided in Appendix D.6.

Baselines. We compare GravMAD against various baselines, covering both foundation model-based and imitation learning-based methods. For the foundation model-based approach, we use **VoxPoser** (Huang et al., 2023) as the baseline. VoxPoser leverages GPT-4 to generate code for constructing value maps, which are then used by a heuristic-based motion planner to synthesize robotic arm trajectories. We reproduce this baseline in our tasks using prompt templates from Huang et al. and our SoM-based Detector, with five camera viewpoints in RLBench. For the imitation learning-based baselines, we select: (1) **3D Diffuser Actor** (Ke et al., 2024), which combines 3D scene representations with a diffusion policy for robotic manipulation tasks. To highlight instruction-following tasks, we use the enhanced language-conditioned version provided by Ke et al.; and (2) **Act3D** (Gervet et al., 2023), which uses a 3D feature field within a policy transformer to represent the robot's workspace. Differences between GravMAD and these baselines are detailed in Appendix A.4.

Training and Evaluation Details. GravMAD runs in a multi-task setting during both the training and testing phases. All models complete 600k training iterations on an NVIDIA RTX4090 GPU, with the final checkpoint selected using three random seeds for evaluation. During testing, except for the novel task *"Push Buttons Light"*, which must be completed within 3 time steps, all other tasks must be finished within 25 time steps; otherwise, they are considered failures. Evaluation metrics include average success rate and rank. The success rate measures the proportion of tasks completed based on language instructions. Meanwhile, the average rank calculates the average of each model's rankings across all tasks, reflecting the model's overall performance in the tasks. Two settings are used for generating context $\mathcal{C}$ during testing: *Manual* and *VLM*. In the manual setting, we manually provide the Detector with the precise 3D coordinates of task-related objects in the simulation to generate accurate context. In the VLM setting, we use a Detector implemented with SoM and GPT-4o to locate task-related objects and generate context.

4.2 GENERALIZATION PERFORMANCE OF GRAVMAD TO NOVEL TASKS

In Table 1, we present the generalization performance of models trained on 12 base tasks when tested on 8 novel tasks, along with visualized trajectories from two of these tasks. The results show that changes in task scenarios and instructions negatively impact the test performance of all pre-trained models to some extent. However, GravMAD exhibits superior generalization across all 8 novel tasks compared to the baseline models. In terms of average success rate, GravMAD outperforms VoxPoser, Act3D, and 3D Diffuser Actor by **28.63%**, **45.09%**, and **33.54%**, respectively. VoxPoser

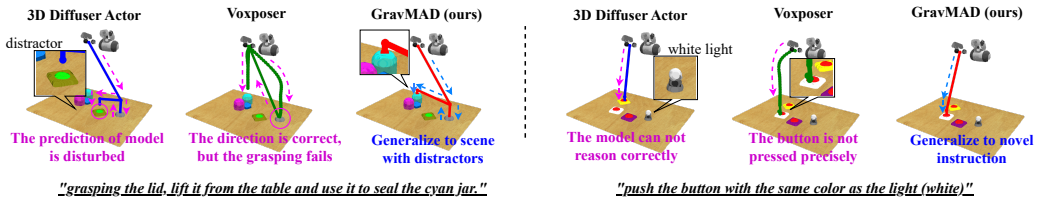

Models	Avg. Success ↑	Avg. Rank ↓	Close Drawer	Close Jar Banana	Close Jar Distractor	Condition Block	Meat On Grill	Open Drawer Small	Stack cups blocks	Push Buttons Light
Voxposer (Huang et al., 2023)	34.29	2.6	96.00 ±4.00	17.33 ±19.73	22.67 ±10.07	25.00 ±23.26	38.67 ±12.22	6.67 ±2.31	0.00 ±0.00	68.00 ±18.33
Act3D (Gervet et al., 2023)	17.83	3.5	66.67±9.24	29.33±9.24	41.33±4.62	0.00±0.00	1.33±2.31	2.67±4.62	0.00±0.00	1.33±2.31
3D Diffuser Actor (Ke et al., 2024)	29.38	2.9	81.33±6.11	48.00±4.00	42.67±4.62	27.00±10.15	0.00±0.00	2.67±4.62	2.67±2.31	30.67±12.86
GravMAD (VLM)	**62.92**	1.0	**97.33**±2.31	**84.00**±00.00	**86.67**±2.31	**74.00**±11.14	**45.33**±4.62	**21.33**±12.86	**18.67**±2.31	**76.00**±8.00
Performance gain	**+28.63**	-	**+1.33**	**+36.00**	**+44.00**	**+47.00**	**+6.66**	**+14.66**	**+16.00**	**+8.00**

Table 1: **Generalization to 8 novel RLBench tasks.** Evaluations on 8 novel tasks are conducted using 3 seeds, with 25 test episodes per task, utilizing the final checkpoints from training on 12 base tasks. Performance gains are compared to the best-performing baselines, indicated by underlines.

Models	Avg. Success ↑	Avg. Rank ↓	Close Jar	Open Drawer	Meat off Grill	Slide Block	Put in Drawer
Voxposer (Huang et al., 2023)	15.11	4.5	12.00±10.58	10.67±8.33	45.33±24.44	0.00±0.00	0.00±0.00
Act3D (Gervet et al., 2023)	34.11	4.3	61.33±4.62	41.33±4.62	60.0±6.92	78.67±2.31	49.33±10.07
3D Diffuser Actor (Ke et al., 2024)	55.81	2.3	66.67±2.31	88.00±6.93	88.00±4.00	84.00±0.00	94.67±2.31
GravMAD (Manual)	**69.17**	1.3	**100.00**±0.00	76.67±4.62	**89.33**±2.31	**93.33**±2.31	78.67±6.11
Performance gain	**+13.36**	-	**+33.33**	-13.33	**+1.33**	**+9.33**	-16.00
GravMAD (VLM)	**56.72**	2.1	**100.00**±0.00	58.67±2.31	70.67±2.31	80.00±0.00	61.33±9.24
Performance gain	**+0.91**	-	**+33.33**	-29.33	-17.33	-4.00	-33.34
Models	**Push Buttons**	**Stack Blocks**	**Place Cups**	**Place Wine**	**Screw Bulb**	**Insert Peg**	**Stack Cups**
Voxposer (Huang et al., 2023)	80.00±13.86	16.00±12.00	6.67±8.33	5.33±2.31	4.00±4.00	0.00±0.00	1.33±2.31
Act3D (Gervet et al., 2023)	66.67±2.31	0.00±0.00	0.00±0.00	45.33±2.31	6.67±2.31	0.00±0.00	0.00±0.00
3D Diffuser Actor (Ke et al., 2024)	94.67±2.31	13.67±2.89	5.33±6.11	82.67±2.31	29.33±2.31	2.67±4.62	20.00±0.00
GravMAD (Manual)	**98.67**±2.31	**56.67**±4.62	5.33±2.31	77.33±4.62	**66.67**±6.11	**32.00**±6.93	**57.33**±2.31
Performance gain	**+4.00**	**+40.67**	-1.34	-5.34	**+37.34**	**+29.33**	**+37.33**
GravMAD (VLM)	**97.33**±2.31	**51.33**±6.11	5.33±4.62	33.33±4.62	**54.67**±6.11	**18.67**±4.62	**49.33**±2.31
Performance gain	**+2.66**	**+35.33**	-1.34	-49.34	**+25.34**	**+16.00**	**+29.33**

Table 2: **Multi-task test results on 12 base tasks.** All models are trained on 12 base tasks with 20 demonstrations each. Final checkpoints are evaluated across 3 seeds with 25 test episodes per task. Performance gains are compared to the best-performing baselines.

leverages large models to achieve a certain level of performance on novel tasks, but its heuristic motion planner fails to grasp object properties and task interaction conditions, leading to poor results on tasks requiring fine manipulation, as shown in the trajectory visualizations. Similarly, 3D Diffuser Actor and Act3D struggle to transfer skills from training to novel tasks, primarily due to overfitting to training-specific tasks, which hampers generalization. In contrast, GravMAD uses VLM-generated GravMaps to guide action diffusion, enabling effective object interaction and strong performance on novel tasks. These results clearly demonstrate GravMAD's superior generalization.

4.3 Test Performance of GravMAD on Base Tasks

Table 2 compares the performance of all models on 12 base tasks. GravMAD (Manual) outperforms Act3D and Voxposer across all tasks and exceeds the best baseline, 3D Diffuser Actor, in 9 out of 12 tasks, with an average success rate improvement of **13.36%**. Despite the Detector's coarse SoM positioning affecting GravMAD (VLM)'s performance, it still outperforms Act3D and Voxposer on all tasks, with a **0.91%** higher average success rate than 3D Diffuser Actor. These results clearly show that GravMAD remains highly competitive even on previously seen tasks. As long as task-related object positions are accurate, the generated GravMap effectively reflects sub-goals and guides action diffusion, enabling precise execution by GravMAD. GravMAD (Manual) underperforms 3D Diffuser Actor in the *"Open Drawer"*, *"Put in Drawer"*, and *"Place Wine"* tasks due to slight deviations between the manually provided object positions and the sub-goals. In high-precision tasks, even small deviations can impact performance. For example, in the *"Open Drawer"* task, the robot needs to grasp the center of the small handle for optimal performance. After manually adjusting the sub-goal to better align with the handle, performance improved. GravMAD (VLM) also struggles in tasks like *"Place Wine"* due to inaccuracies in the object positions provided by the Detector, especially when Semantic SAM fails to provide precise locations or the camera doesn't capture the full scene. For further analysis of failure cases, please refer to Appendix B.3.

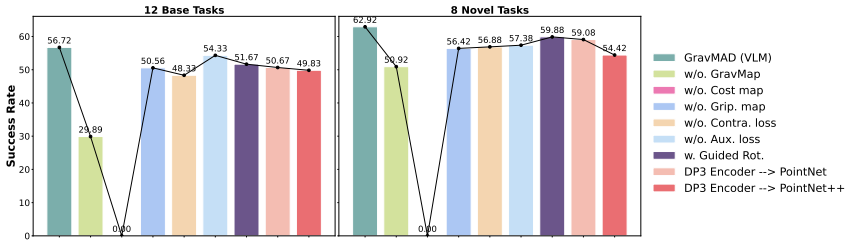

Figure 4: **Ablation Studies**. We evaluate the impact of key design elements by reporting the average success rates across 12 base tasks and 8 novel tasks. In the results, "→" denotes replacement, "w/o" indicates "without", and "w." signifies "with".

4.4 Ablations

Extensive ablation studies are conducted to analyze the role of each key design element in GravMAD, with the results shown in Fig 4. The following findings are revealed: **1) Impact of replacing GravMaps with specific sub-goal position and openness**: Replacing GravMaps with sub-goals g^{pos} and g^{open} (w/o GravMap) results in a significant performance drop. Without GravMaps, the policy lacks regional context, becoming overly sensitive to precise positions and unable to generalize to slight spatial variations. **2) Importance of both cost map and gripper map in GravMaps**: The combination of the cost map and gripper map within GravMaps is essential for guiding the model's attention to sub-goal locations and ensuring effective gripper usage. The absence of the gripper map causes a moderate decline in performance (w/o. Grip. map). In contrast, omitting the cost map causes zero-gradient issues during training, leading to incorrect predictions and task failure. This occurs because the encoder cannot process such input. Additional experiments for this ablation, detailed in Appendix D.5, highlight the cost map's impact on performance. (w/o. Cost map) **3) Significance of contrastive learning loss and auxiliary losses**: Removing the contrastive learning loss $\mathcal{L}_{\text{con}}$ results in highly similar features from the point cloud encoder, diminishing their effectiveness in action denoising and leading to a decline in model performance (w/o. Contra. loss). Similarly, the absence of auxiliary losses $\mathcal{L}_{\text{aux\_pos}}$ and $\mathcal{L}_{\text{aux\_open}}$ weakens the model's focus on sub-goals, leading to a noticeable drop in performance (w/o Aux. loss). **4) Effect of GravMap tokens on guiding rotation actions:** Conditioning rotation actions with GravMap tokens in the action diffusion process results in a performance drop, likely due to the inherent nature of rotation actions, which makes them difficult to be guided explicitly through value maps (w. Guided Rot.). **5) Impact of different point cloud encoders on GravMap performance.** Replacing the DP3 encoder in GravMAD with PointNet (Qi et al., 2017a) (DP3 Encoder → PointNet) or PointNet++ (Qi et al., 2017b) (DP3 Encoder → PointNet++) leads to a performance decline. We suspect that lightweight encoders help prevent overfitting to training data details, enhancing GravMAD's generalization ability across different tasks or unseen data.

5 Conclusion and Discussion

In this paper, we introduce GravMAD, a novel action diffusion framework that facilitates generalized 3D manipulation using sub-goals. GravMAD grounds language instructions into spatial subgoals within the 3D workspace through grounded spatial value maps (GravMaps). During training, these GravMaps are generated from demonstrations by Sub-goal Keyposes Discovery . In the inference phase, GravMaps are constructed by leveraging foundational models to directly predict sub-goals. Consequently, GravMAD seamlessly integrates the precision of imitation learning with the strong generalization capabilities of foundational models, leading to superior performance across a variety of manipulation tasks. Extensive experiments on the RLBench benchmark and real-robot tasks show that GravMAD achieves competitive performance on training tasks. It also generalizes well to novel tasks, demonstrating its potential for practical use across diverse 3D environments. Despite its promising results, GravMAD has some limitations. First, its effectiveness relies heavily on prompt engineering, which can be challenging for inexperienced users. Additionally, the visual-language models (VLMs) have limited detection capabilities and are sensitive to changes in camera perspective, affecting performance and preventing optimal efficiency and accuracy. Future work will address these issues to enhance the model's performance, expand its applicability, and validate its use on more complex and long-horizon real-robot tasks.

REFERENCES

Brenna D. Argall, Sonia Chernova, Manuela M. Veloso, and Brett Browning. A survey of robot learning from demonstration. *Robotics Auton. Syst.*, 57(5):469–483, 2009.

Kevin Black, Mitsuhiko Nakamoto, Pranav Atreya, Homer Rich Walke, Chelsea Finn, Aviral Kumar, and Sergey Levine. Zero-shot robotic manipulation with pre-trained image-editing diffusion models. In *International Conference on Learning Representations (ICLR)*, 2024.

Anthony Brohan, Noah Brown, Justice Carbajal, Yevgen Chebotar, Joseph Dabis, Chelsea Finn, Keerthana Gopalakrishnan, Karol Hausman, Alexander Herzog, Jasmine Hsu, Julian Ibarz, Brian Ichter, Alex Irpan, Tomas Jackson, Sally Jesmonth, Nikhil J. Joshi, Ryan Julian, Dmitry Kalashnikov, Yuheng Kuang, Isabel Leal, Kuang-Huei Lee, Sergey Levine, Yao Lu, Utsav Malla, Deeksha Manjunath, Igor Mordatch, Ofir Nachum, Carolina Parada, Jodilyn Peralta, Emily Perez, Karl Pertsch, Jornell Quiambao, Kanishka Rao, Michael S. Ryoo, Grecia Salazar, Pannag R. Sanketi, Kevin Sayed, Jaspiar Singh, Sumedh Sontakke, Austin Stone, Clayton Tan, Huong T. Tran, Vincent Vanhoucke, Steve Vega, Quan Vuong, Fei Xia, Ted Xiao, Peng Xu, Sichun Xu, Tianhe Yu, and Brianna Zitkovich. RT-1: robotics transformer for real-world control at scale. In *Proceedings of Robotics: Science and Systems (RSS)*, 2023a.

Anthony Brohan, Yevgen Chebotar, Chelsea Finn, Karol Hausman, Alexander Herzog, Daniel Ho, Julian Ibarz, Alex Irpan, Eric Jang, Ryan Julian, et al. Do as i can, not as i say: Grounding language in robotic affordances. In *Conference on robot learning (CoRL)*, pp. 287–318. PMLR, 2023b.

Shizhe Chen, Ricardo Garcia Pinel, Cordelia Schmid, and Ivan Laptev. Polarnet: 3d point clouds for language-guided robotic manipulation. In *Conference on Robot Learning (CoRL)*, pp. 1761–1781. PMLR, 2023.

Danny Driess, Fei Xia, Mehdi S. M. Sajjadi, Corey Lynch, Aakanksha Chowdhery, Brian Ichter, Ayzaan Wahid, Jonathan Tompson, Quan Vuong, Tianhe Yu, Wenlong Huang, Yevgen Chebotar, Pierre Sermanet, Daniel Duckworth, Sergey Levine, Vincent Vanhoucke, Karol Hausman, Marc Toussaint, Klaus Greff, Andy Zeng, Igor Mordatch, and Pete Florence. Palm-e: An embodied multimodal language model. In Andreas Krause, Emma Brunskill, Kyunghyun Cho, Barbara Engelhardt, Sivan Sabato, and Jonathan Scarlett (eds.), *International Conference on Machine Learning (ICML)*, volume 202, pp. 8469–8488. PMLR, 2023.

Ricardo Garcia, Shizhe Chen, and Cordelia Schmid. Towards generalizable vision-language robotic manipulation: A benchmark and llm-guided 3d policy. *arXiv preprint arXiv:2410.01345*, 2024.

Theophile Gervet, Zhou Xian, Nikolaos Gkanatsios, and Katerina Fragkiadaki. Act3d: 3d feature field transformers for multi-task robotic manipulation. In *Conference on Robot Learning (CoRL)*, pp. 3949–3965. PMLR, 2023.

Ankit Goyal, Jie Xu, Yijie Guo, Valts Blukis, Yu-Wei Chao, and Dieter Fox. Rvt: Robotic view transformer for 3d object manipulation. In *Conference on Robot Learning (CoRL)*, pp. 694–710. PMLR, 2023.

Ankit Goyal, Valts Blukis, Jie Xu, Yijie Guo, Yu-Wei Chao, and Dieter Fox. Rvt2: Learning precise manipulation from few demonstrations. *Proceedings of Robotics: Science and Systems (RSS)*, 2024.

Jonathan Ho, Ajay Jain, and Pieter Abbeel. Denoising diffusion probabilistic models. *Advances in neural information processing systems (NeurIPS)*, 33:6840–6851, 2020.

Yafei Hu, Quanting Xie, Vidhi Jain, Jonathan Francis, Jay Patrikar, Nikhil Keetha, Seungchan Kim, Yaqi Xie, Tianyi Zhang, Zhibo Zhao, et al. Toward general-purpose robots via foundation models: A survey and meta-analysis. *arXiv preprint arXiv:2312.08782*, 2023a.

Yingdong Hu, Fanqi Lin, Tong Zhang, Li Yi, and Yang Gao. Look before you leap: Unveiling the power of gpt-4v in robotic vision-language planning. *arXiv preprint arXiv:2311.17842*, 2023b.

Haoxu Huang, Fanqi Lin, Yingdong Hu, Shengjie Wang, and Yang Gao. Copa: General robotic manipulation through spatial constraints of parts with foundation models. *arXiv preprint arXiv:2403.08248*, 2024.

Wenlong Huang, Pieter Abbeel, Deepak Pathak, and Igor Mordatch. Language models as zero-shot planners: Extracting actionable knowledge for embodied agents. In *International Conference on Machine Learning (ICML)*, pp. 9118–9147. PMLR, 2022.

Wenlong Huang, Chen Wang, Ruohan Zhang, Yunzhu Li, Jiajun Wu, and Li Fei-Fei. Voxposer: Composable 3d value maps for robotic manipulation with language models. In *Conference on Robot Learning (CoRL)*, pp. 540–562. PMLR, 2023.

Stephen James and Andrew J Davison. Q-attention: Enabling efficient learning for vision-based robotic manipulation. *IEEE Robotics and Automation Letters*, 7(2):1612–1619, 2022.

Stephen James, Zicong Ma, David Rovick Arrojo, and Andrew J. Davison. Rlbench: The robot learning benchmark & learning environment. *IEEE Robotics and Automation Letter*, 5(2):3019–3026, 2020a.

Stephen James, Zicong Ma, David Rovick Arrojo, and Andrew J Davison. Rlbench: The robot learning benchmark & learning environment. *IEEE Robotics and Automation Letters*, 5(2):3019–3026, 2020b.

Stephen James, Kentaro Wada, Tristan Laidlow, and Andrew J Davison. Coarse-to-fine q-attention: Efficient learning for visual robotic manipulation via discretisation. In *Proceedings of the IEEE/CVF Conference on Computer Vision and Pattern Recognition (CVPR)*, pp. 13739–13748, 2022.

Eric Jang, Alex Irpan, Mohi Khansari, Daniel Kappler, Frederik Ebert, Corey Lynch, Sergey Levine, and Chelsea Finn. Bc-z: Zero-shot task generalization with robotic imitation learning. In *Conference on Robot Learning (CoRL)*, pp. 991–1002. PMLR, 2022.

Xuhui Kang, Wenqian Ye, and Yen-Ling Kuo. Imagined subgoals for hierarchical goal-conditioned policies. In *CoRL 2023 Workshop on Learning Effective Abstractions for Planning (LEAP)*, 2023.

Tsung-Wei Ke, Nikolaos Gkanatsios, and Katerina Fragkiadaki. 3d diffuser actor: Policy diffusion with 3d scene representations. In *Conference on Robot Learning (CoRL)*. PMLR, 2024.

Sebastian Klemm, Jan Oberländer, Andreas Hermann, Arne Roennau, Thomas Schamm, J Marius Zollner, and Rüdiger Dillmann. Rrt*-connect: Faster, asymptotically optimal motion planning. In *2015 IEEE international conference on robotics and biomimetics (ROBIO)*, pp. 1670–1677. IEEE, 2015.

Feng Li, Hao Zhang, Peize Sun, Xueyan Zou, Shilong Liu, Jianwei Yang, Chunyuan Li, Lei Zhang, and Jianfeng Gao. Semantic-sam: Segment and recognize anything at any granularity. *arXiv preprint arXiv:2307.04767*, 2023.

Xinghang Li, Minghuan Liu, Hanbo Zhang, Cunjun Yu, Jie Xu, Hongtao Wu, Chilam Cheang, Ya Jing, Weinan Zhang, Huaping Liu, Hang Li, and Tao Kong. Vision-language foundation models as effective robot imitators. In *International Conference on Learning Representations (ICLR)*, 2024.

Jacky Liang, Wenlong Huang, Fei Xia, Peng Xu, Karol Hausman, Brian Ichter, Pete Florence, and Andy Zeng. Code as policies: Language model programs for embodied control. In *IEEE International Conference on Robotics and Automation (ICRA)*, pp. 9493–9500. IEEE, 2023.

Xiao Ma, Sumit Patidar, Iain Haughton, and Stephen James. Hierarchical diffusion policy for kinematics-aware multi-task robotic manipulation. In *Proceedings of the IEEE/CVF Conference on Computer Vision and Pattern Recognition (CVPR)*, pp. 18081–18090, 2024.

OpenAI. GPT-4 technical report. *CoRR*, abs/2303.08774, 2023.

Abhishek Padalkar, Ajinkya Jain, Alex Bewley, Alexander Herzog, Alex Irpan, Alexander Khazatsky, Anant Raj, Anikait Singh, Anthony Brohan, Antonin Raffin, Ayzaan Wahid, Ben Burgess-Limerick, Beomjoon Kim, Bernhard Schölkopf, Brian Ichter, Cewu Lu, Charles Xu, Chelsea Finn, Chenfeng Xu, Cheng Chi, Chenguang Huang, Christine Chan, Chuer Pan, Chuyuan Fu, Coline Devin, Danny Driess, Deepak Pathak, Dhruv Shah, Dieter Büchler, Dmitry Kalashnikov, Dorsa Sadigh, Edward Johns, Federico Ceola, Fei Xia, Freek Stulp, Gaoyue Zhou, Gaurav S. Sukhatme, Gautam

Salhotra, Ge Yan, Giulio Schiavi, Gregory Kahn, Hao Su, Haoshu Fang, Haochen Shi, Heni Ben Amor, Henrik I. Christensen, Hiroki Furuta, Homer Walke, Hongjie Fang, Igor Mordatch, Ilija Radosavovic, and et al. Open x-embodiment: Robotic learning datasets and RT-X models. In *IEEE International Conference on Robotics and Automation (ICRA)*, pp. 6892–6903. IEEE, 2024.

Ethan Perez, Florian Strub, Harm De Vries, Vincent Dumoulin, and Aaron Courville. Film: Visual reasoning with a general conditioning layer. In *Proceedings of the AAAI conference on artificial intelligence (AAAI)*, 2018.

Charles R Qi, Hao Su, Kaichun Mo, and Leonidas J Guibas. Pointnet: Deep learning on point sets for 3d classification and segmentation. In *Proceedings of the IEEE/CVF Conference on Computer Vision and Pattern Recognition (CVPR)*, pp. 652–660, 2017a.

Charles Ruizhongtai Qi, Li Yi, Hao Su, and Leonidas J Guibas. Pointnet++: Deep hierarchical feature learning on point sets in a metric space. *Advances in neural information processing systems (NeurIPS)*, 30, 2017b.

Alec Radford, Jong Wook Kim, Chris Hallacy, Aditya Ramesh, Gabriel Goh, Sandhini Agarwal, Girish Sastry, Amanda Askell, Pamela Mishkin, Jack Clark, et al. Learning transferable visual models from natural language supervision. In *International Conference on Machine Learning (ICML)*, pp. 8748–8763. PMLR, 2021.

SP Sharan, Ruihan Zhao, Zhangyang Wang, Sandeep P Chinchali, et al. Plan diffuser: Grounding llm planners with diffusion models for robotic manipulation. In *Bridging the Gap between Cognitive Science and Robot Learning in the Real World: Progresses and New Directions*, 2024.

Mohit Shridhar, Lucas Manuelli, and Dieter Fox. Perceiver-actor: A multi-task transformer for robotic manipulation. In *Conference on Robot Learning (CoRL)*, pp. 785–799. PMLR, 2023.

Mohit Shridhar, Yat Long Lo, and Stephen James. Generative image as action models. In *8th Annual Conference on Robot Learning (CoRL)*, 2024.

Homer Rich Walke, Kevin Black, Tony Z. Zhao, Quan Vuong, Chongyi Zheng, Philippe Hansen-Estruch, Andre Wang He, Vivek Myers, Moo Jin Kim, Max Du, Abraham Lee, Kuan Fang, Chelsea Finn, and Sergey Levine. Bridgedata V2: A dataset for robot learning at scale. In Jie Tan, Marc Toussaint, and Kourosh Darvish (eds.), *Conference on Robot Learning (CoRL)*, volume 229, pp. 1723–1736. PMLR, 2023.

Zhou Xian, Nikolaos Gkanatsios, Theophile Gervet, Tsung-Wei Ke, and Katerina Fragkiadaki. Chaineddiffuser: Unifying trajectory diffusion and keypose prediction for robotic manipulation. In *Conference on Robot Learning (CoRL)*, pp. 2323–2339. PMLR, 2023.

Annie Xie, Lisa Lee, Ted Xiao, and Chelsea Finn. Decomposing the generalization gap in imitation learning for visual robotic manipulation. In *IEEE International Conference on Robotics and Automation (ICRA)*, pp. 3153–3160. IEEE, 2024.

Ge Yan, Yueh-Hua Wu, and Xiaolong Wang. Dnact: Diffusion guided multi-task 3d policy learning. *arXiv preprint arXiv:2403.04115*, 2024.

Jianwei Yang, Hao Zhang, Feng Li, Xueyan Zou, Chunyuan Li, and Jianfeng Gao. Set-of-mark prompting unleashes extraordinary visual grounding in GPT-4V. *CoRR*, abs/2310.11441, 2023a.

Zhengyuan Yang, Linjie Li, Kevin Lin, Jianfeng Wang, Chung-Ching Lin, Zicheng Liu, and Lijuan Wang. The dawn of lmms: Preliminary explorations with gpt-4v(ision). *CoRR*, abs/2309.17421, 2023b.

Yida Yin, Zekai Wang, Yuvan Sharma, Dantong Niu, Trevor Darrell, and Roei Herzig. In-context learning enables robot action prediction in llms. *arXiv preprint arXiv:2410.12782*, 2024.

Wentao Yuan, Adithyavairavan Murali, Arsalan Mousavian, and Dieter Fox. M2t2: Multi-task masked transformer for object-centric pick and place. In *Conference on Robot Learning (CoRL)*, pp. 3619–3630. PMLR, 2023.

Yanjie Ze, Ge Yan, Yueh-Hua Wu, Annabella Macaluso, Yuying Ge, Jianglong Ye, Nicklas Hansen, Li Erran Li, and Xiaolong Wang. Gnfactor: Multi-task real robot learning with generalizable neural feature fields. In Jie Tan, Marc Toussaint, and Kourosh Darvish (eds.), *Conference on Robot Learning (CoRL)*, volume 229, pp. 284–301. PMLR, 2023.

Yanjie Ze, Gu Zhang, Kangning Zhang, Chenyuan Hu, Muhan Wang, and Huazhe Xu. 3d diffusion policy: Generalizable visuomotor policy learning via simple 3d representations. In *Proceedings of Robotics: Science and Systems (RSS)*, 2024.

Junjie Zhang, Chenjia Bai, Haoran He, Zhigang Wang, Bin Zhao, Xiu Li, and Xuelong Li. Sam-e: Leveraging visual foundation model with sequence imitation for embodied manipulation. In *International Conference on Machine Learning (ICML)*, 2024.

Tong Zhang, Yingdong Hu, Hanchen Cui, Hang Zhao, and Yang Gao. A universal semantic-geometric representation for robotic manipulation. In *Conference on Robot Learning (CoRL)*, pp. 3342–3363. PMLR, 2023.

Hongkuan Zhou, Xiangtong Yao, Yuan Meng, Siming Sun, Zhenshan BIng, Kai Huang, and Alois Knoll. Language-conditioned learning for robotic manipulation: A survey. *arXiv preprint arXiv:2312.10807*, 2023.

Brianna Zitkovich, Tianhe Yu, Sichun Xu, Peng Xu, Ted Xiao, Fei Xia, Jialin Wu, Paul Wohlhart, Stefan Welker, Ayzaan Wahid, Quan Vuong, Vincent Vanhoucke, Huong T. Tran, Radu Soricut, Anikait Singh, Jaspiar Singh, Pierre Sermanet, Pannag R. Sanketi, Grecia Salazar, Michael S. Ryoo, Krista Reymann, Kanishka Rao, Karl Pertsch, Igor Mordatch, Henryk Michalewski, Yao Lu, Sergey Levine, Lisa Lee, Tsang-Wei Edward Lee, Isabel Leal, Yuheng Kuang, Dmitry Kalashnikov, Ryan Julian, Nikhil J. Joshi, Alex Irpan, Brian Ichter, Jasmine Hsu, Alexander Herzog, Karol Hausman, Keerthana Gopalakrishnan, Chuyuan Fu, Pete Florence, Chelsea Finn, Kumar Avinava Dubey, Danny Driess, Tianli Ding, Krzysztof Marcin Choromanski, Xi Chen, Yevgen Chebotar, Justice Carbajal, Noah Brown, Anthony Brohan, Montserrat Gonzalez Arenas, and Kehang Han. RT-2: vision-language-action models transfer web knowledge to robotic control. In *Conference on Robot Learning (CoRL)*, volume 229, pp. 2165–2183. PMLR, 2023.

A Additional Implementation Details

A.1 Heuristics for Sub-goal Keypose Discovery

Building on keypose discovery (James & Davison, 2022), we propose the Sub-goal Keypose Discovery method to identify sub-goal keyposes from demonstrations, focusing on changes in the gripper's state and touch forces. This is particularly relevant for object manipulation tasks, where the robot's interactions with objects can be segmented into discrete sub-goals.

The implementation of the Sub-goal Keypose Discovery algorithm starts with a set of pre-computed keyposes, which are frames selected from the demonstration sequence through an initial keypose discovery process. We introduce two functions: `touch_change`, shown in Algorithm 2, and `gripper_change`, shown in Algorithm 3, to evaluate whether a keypose qualifies as a sub-goal. The first function checks for significant changes in the gripper's touch forces, while the second evaluates changes in the gripper's open/close state. The pseudocode in Algorithm 4 outlines the heuristic steps for identifying sub-goal keyposes.

One current limitation of the Sub-goal Keypose Discovery method is its inability to effectively handle tasks involving tool use, which we plan to address in future research.

Algorithm 2: touch_change Function

Input: Demonstration sequence *demo*, Keypose index *k*, Threshold *touch_threshold*, Tolerance *delta*
Output: Boolean indicating significant touch force change
begin
  Set *start* to max(0, *k* - *touch_threshold*);
  for *each index j from start to k-1* **do**
    if *Touch forces at j differ from Touch forces at k within tolerance delta* **then**
      return *True*;
  return *False*;

Algorithm 3: gripper_change Function

Input: Demonstration sequence *demo*, Keypose index *k*, Threshold *gripper_threshold*
Output: Boolean indicating gripper state change
begin
  Set *start* to max(0, *k* - *gripper_threshold*);
  for *each index j from start to k-1* **do**
    if *Gripper state at j differs from Gripper state at k* **then**
      return *True*;
  return *False*;

A.2 Details of GravMap Synthesis

A.2.1 Training Phase

To facilitate GravMap synthesis, we assign a goal action to each keypose by linking it to the action performed at the nearest future sub-goal. This association enables us to determine the relevant cost and gripper state for different regions of the GravMap. In the first map, $m_c \in \mathbb{R}^{w \times h \times d}$, the cost is lower near the positions of the robotic end-effector at these sub-goal keyposes and higher as the distance increases. In the second map, $m_o \in \mathbb{R}^{w \times h \times d}$, areas near the end-effector's position at the sub-goal keyposes reflect the gripper state at the sub-goal, while other areas reflect the gripper state at the current frame.

Algorithm 4: Heuristics for Sub-goal Keypose Discovery

Input: Demonstration sequence *demo*, Task type *task_str*, Threshold parameters *touch_threshold, gripper_threshold, delta*
Output: List of sub-goal keyposes *sub_goal_keyposes*
begin
  Initialize *sub_goal_keyposes* as an empty list;
  Identify keyposes from *demo* using keypose discovery method;
  for *each keypose k in keyposes* **do**
    if *task_str is a task involving touch without grasping* **then**
      if ***touch_change****(demo, k, touch_threshold, delta)* **then**
        Append *k* to *sub_goal_keyposes*;
    else
      if ***gripper_change****(demo, k, gripper_threshold)* ***or touch_change****(demo, k, touch_threshold, delta)* **then**
        Append *k* to *sub_goal_keyposes*;
  Append the last keypose to *sub_goal_keyposes*;
  return *sub_goal_keyposes*;

Algorithm 5: GravMap Generation

Input: Instruction ℓ, Observed RGB Image $\mathcal{O}$
Prompt : Prompt for Detector $\mathcal{P}_{\text{det}}$, Prompt for Planner $\mathcal{P}_{\text{plan}}$, Prompt for Composer $\mathcal{P}_{\text{com}}$, Few-shot task specified prompt $\mathcal{P}_{\text{task}} = \{\mathcal{P}'_{\text{det}}, \mathcal{P}'_{\text{plan}}, \mathcal{P}'_{\text{com}}\}$, Cost Map Prompt $\mathcal{P}_{\text{cost}}$, Gripper Map Prompt $\mathcal{P}_{\text{gripper}}$
Output: GravMap m
begin
  $\mathcal{O}' \leftarrow$ Semantic-SAM($\mathcal{O}$); `// Label objects with numerical tags`
  $\mathcal{C} \leftarrow$ Detector($\ell, \mathcal{O}', \mathcal{P}_{\text{det}}, \mathcal{P}'_{\text{det}}$); `// Select relevant objects and get corresponding 3D positions as context`
  $ST \leftarrow$ Planner($\ell, \mathcal{C}, \mathcal{P}_{\text{plan}}, \mathcal{P}'_{\text{plan}}$); `// Infer sub-tasks` $ST = (st_1, st_2, \ldots, st_i)$
  Function calls, parameters $\leftarrow$ Composer($ST, \mathcal{C}, \mathcal{P}_{\text{com}}, \mathcal{P}'_{\text{com}}$); `// Generate API calls and their parameters for generating` g^{pos} `and` g^{open}
  $g^{\text{pos}} \leftarrow$ get_cost_map(Function calls, parameters, $\mathcal{P}_{\text{cost}}$);
  $g^{\text{open}} \leftarrow$ get_gripper_map(Function calls, parameters, $\mathcal{P}_{\text{gripper}}$);
  $m \leftarrow$ GravMap generator(cat($g^{\text{pos}}, g^{\text{open}}$);
  return m;

A.2.2 Inference Phase

In this section, we introduce the complete pipeline for GravMap generation, as outlined in Algorithm 5. This includes Algorithm 1, which details the process of generating a GravMap from a language instruction ℓ and an observed RGB image $\mathcal{O}$. The GravMap generation pipeline integrates VLMs to interpret instructions, ground them in the visual context, and translate them into coarse 3D voxel representations, i.e., the GravMap.

Our pipeline consists of the following three components:

- **Detector.** Starting with an instruction ℓ and an observed RGB image $\mathcal{O}$, the RGB image is passed through the Semantic-SAM segmentation model, which labels each object with a numerical tag, producing a labeled image $\mathcal{O}'$. The GPT4o-based Detector uses the prompts $\mathcal{P}_{\text{det}}$ and $\mathcal{P}'_{\text{det}}$ (adapted from Huang et al. (2024)) to select relevant objects and obtain their 3D positions. The output is a set of selected objects, or context $\mathcal{C}$, which includes the objects' identities and their spatial coordinates in the 3D environment. In the VLM setting, the Detector accesses initial RGB images from four views: wrist, left shoulder, right shoulder,

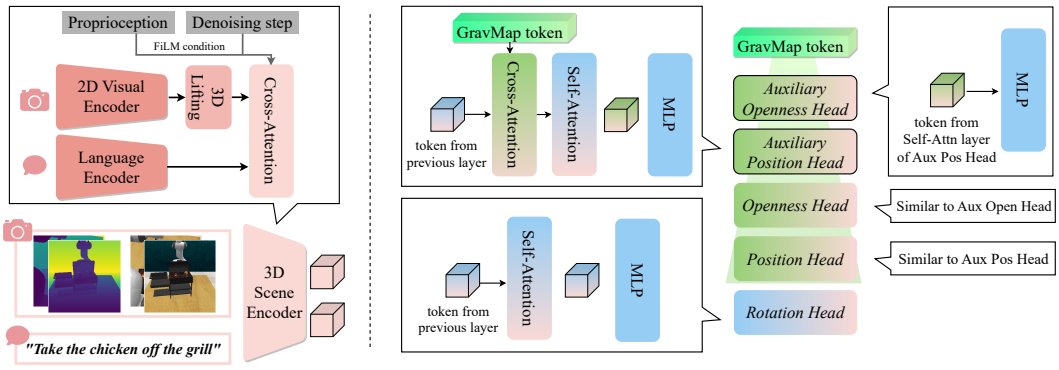

Figure 5: **Detailed description of the modules in GravMAD**, including the 3D Scene Encoder and the prediction heads

and front camera. In the manual setting, precise 3D object attributes are provided from the simulation.

- **Planner.** The GPT4o-based Planner takes the instruction ℓ, context $\mathcal{C}$, and planner-specific prompts $\mathcal{P}_{\text{plan}}$ and $\mathcal{P}'_{\text{plan}}$ (adapted from Huang et al. (2023)) to infer a sequence of sub-tasks $(st_1, st_2, \ldots, st_i)$. Each sub-task describes an action or interaction needed to fulfill the instruction ℓ. Progress is tracked based on the robot's gripper state (open/closed) and whether it is holding an object. The current sub-task is then passed to the Composer for further processing.
- **Composer.** Following Huang et al. (2023), the GPT4o-based Composer parses each inferred sub-task st_i using corresponding prompts $\mathcal{P}_{\text{com}}$ and $\mathcal{P}'_{\text{com}}$. The Composer generates the sub-goal position g^{pos} and sub-goal openness g^{open} by recursively generating code. This includes calls to `get_cost_map` and `get_gripper_map`, which are triggered by cost map prompt $\mathcal{P}_{\text{cost}}$ and gripper map prompt $\mathcal{P}_{\text{gripper}}$. For example, for a sub-task like "push close the topmost drawer," the Composer might generate: `get_cost_map('a point 30cm into the topmost drawer handle')` and `get_gripper_map('close everywhere')`. Natural language parameters are parsed by GPT to generate code that assigns values to g^{pos} and g^{open}. The final GravMap generator in Algorithm 1 then processes g^{pos} and g^{open} to generate the GravMap m.

The prompts mentioned above can be found on the website: `https://gravmad.github.io`.

A.3 Detail of Model Architecture and Hyper-parameters for GravMAD

The detailed hyperparameters of GravMAD are listed in Table 3. Additionally, Fig. 5 provides a detailed overview of GravMAD's modules, including the 3D Scene Encoder and the prediction heads.

(a) The 3D Scene Encoder processes visual and language information separately, merging them via a cross-attention mechanism, with proprioception integrated through FiLM. This allows the model to understand tasks like *"Take the chicken off the grill"* in a 3D environment. First, the visual input is processed by a 2D Visual Encoder, transforming image data into feature representations. These 2D features are then passed through a 3D lifting module, converting them into 3D representations using depth information. Simultaneously, the language input, such as the instruction *"Take the chicken off the grill"*, is encoded into language tokens by the Language Encoder. Finally, the 3D visual features and language tokens are combined through cross-attention, producing 3D Scene tokens.

(b) Each prediction head consists of Attention layers and an MLP. The Auxiliary Position Head receives tokens from the previous layer, which first go through cross-attention with GravMap tokens, followed by self-attention to refine the features. The tokens are then passed through an MLP to output the sub-goal end-effector position. Similarly, the Auxiliary Openness Head takes tokens from the self-attention layer of the Auxiliary Position Head and uses an MLP to predict the sub-goal gripper openness. The Position Head follows the same process as the Auxiliary Position Head, while the

	Values
Sub-goal Keypose Discovery	
touch_threshold	2
Tolerance: delta	0.005
gripper_threshold	4
GravMap	
map_size: S_m	100
offset_range: β_o	3
radius: β_r	3
downsample ratio: β_d	4
number of sampled points: N_p	1024
Model	
image_size	256
token_dim	120
diffusion_timestep	100
noise_scheduler: position	scaled_linear
noise_scheduler: rotation	squaredcos
action_space	absolute pose
Train	
batch_size	8
optimizer	Adam
train_iters	600K
learning_rate	$1e^{-4}$
weight_decay	$5e^{-4}$
loss weight: ω_1	30
loss weight: ω_2	10
loss weight: ω_3	30
loss weight: ω_4	10
Evaluation	
maximal step except push_button_light	25
maximal step of push_button_light	3

Table 3: **Hyper-parameters for GravMAD**, including Sub-goal Keypose Discovery, GravMap, model configuration, training, and evaluation.

Openness Head mirrors the Auxiliary Openness Head. The Rotation Head processes tokens with self-attention and an MLP to predict rotation error.

A.4 Comparison between GravMAD and other baseline models

We compare GravMAD with Voxposer (Huang et al., 2023) and 3D Diffuser Actor (Ke et al., 2024) in Fig. 6.

(a) Voxposer. We describe our reproduction of Voxposer on RLBench. Voxposer uses our SOM-driven Detector to process the input observation and instruction, generating context information. The Planner then receives this context and outputs a sub-goal, representing an intermediate step necessary for the overall motion plan. The Composer processes this sub-goal, producing three maps: Cost Map, Rotation Map, and Gripper Map. These maps guide the robot's movement toward the target in the environment. Note that Voxposer's testing process involves a different number of steps compared to 3D Diffuser Actor and GravMAD, completing only after all LLM inferences are executed.

(b) 3D Diffuser Actor. We use the language-enhanced version of 3D Diffuser Actor as a baseline. 3D Diffuser employs a 3D Scene Encoder to transform visual and language inputs into 3D Scene tokens, providing an understanding of the 3D environment. An MLP encodes noisy estimates of position and rotation into corresponding tokens, which are then fed, along with the 3D Scene tokens, into a denoising network for action diffusion. This network, conditioned on proprioception and the denoising step, includes attention layers, Openness Head, Position Head, and Rotation Head. During diffusion, noisy position/rotation tokens attend to 3D Scene tokens, and cross-attention with instruction tokens enhances language understanding. These instruction tokens are also used in the prediction processes of the Openness, Position, and Rotation heads.

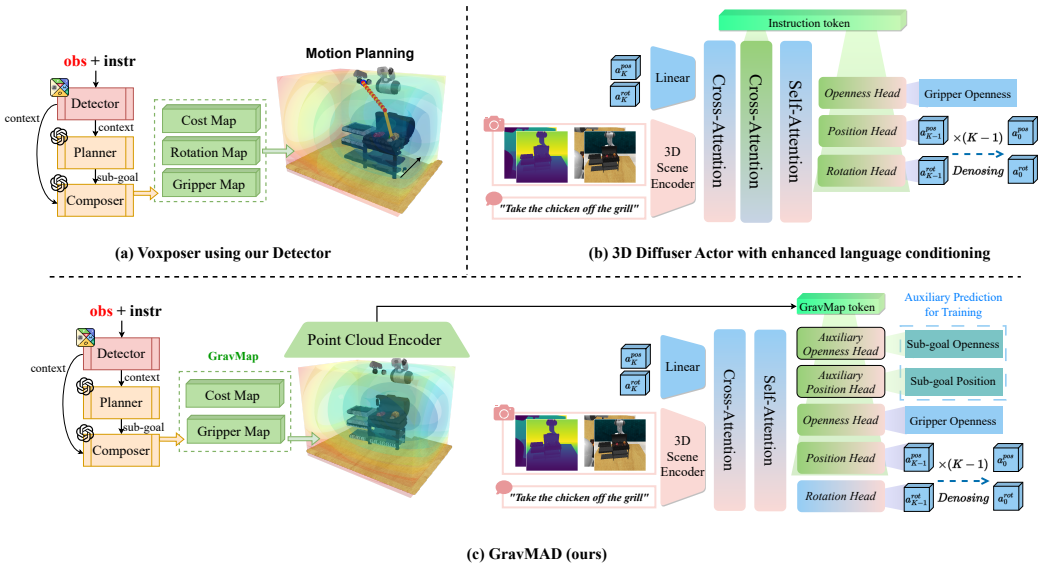

Figure 6: **Comparison of GravMAD with Voxposer and 3D Diffuser Actor**. Unlike Voxposer, which uses planning, GravMAD leverages GravMaps for learning. Compared to 3D Diffuser Actor, GravMAD employs GravMap tokens to guide the action diffusion process and introduces auxiliary position and openness heads to improve representation learning.

(c) GravMAD (ours). GravMAD shares components with Voxposer, such as the Detector, Planner, and Composer, but incorporates task-specific prompt engineering. Unlike Voxposer, which uses maps for planning, GravMAD encodes these maps into tokens using a point cloud encoder, which are then employed in the action diffusion process. Compared to 3D Diffuser Actor, the key difference is that GravMAD uses GravMap tokens instead of language tokens, improving generalization. Additionally, GravMAD introduces two auxiliary tasks to predict sub-goals, enhancing representation learning.

B Additional Experimental Details

B.1 Base Task

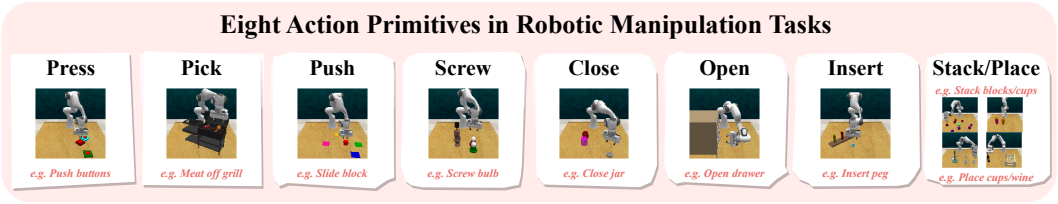

Figure 7: Eight action primitives in robotic manipulation tasks.

For the selection of base tasks, our primary criterion is to ensure they comprehensively cover the fundamental action primitives in robotic manipulation tasks. Therefore, we follow Garcia et al. (2024) and further summarize the eight essential action primitives required for robotic manipulation, as shown in Fig. 7. In line with this criterion, we select 12 base tasks from RLBench (James et al., 2020a), as illustrated in Fig. 8. These 12 tasks also include short-term tasks (*close jar, open drawer, meat off grill, slide block, push buttons, place wine*), long-horizon tasks (*put item in drawer, stack blocks, stack cups*), and tasks that require high-precision manipulation (*screw bulb, insert peg, place cups*). Each base task contains 2 to 60 variants in the instructions, covering differences in color, placement, category, and count. In addition to instruction variations, the objects, distractors, and their positions and scenes are randomly initialized in the environment. The templates representing task

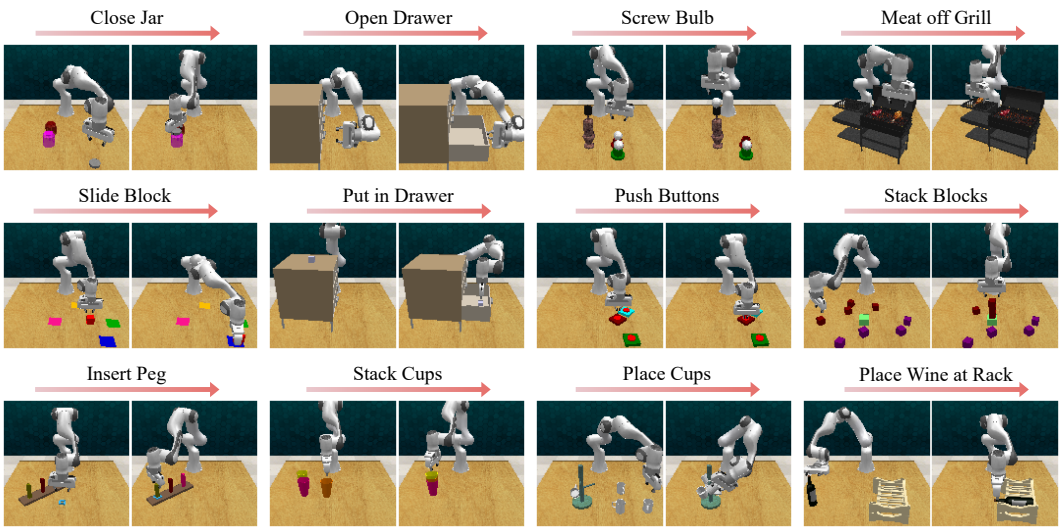

Figure 8: Visualization of 12 base tasks.

Table 4: The 12 base tasks selected from RLBench (James et al., 2020a)

Task	Variation Type	# of Variations	Avg. Keyposes	Language Template
close jar	color	20	6.0	"close the — jar"
open drawer	placement	3	3.0	"open the — drawer"
screw bulb	color	20	7.0	"screw in the — light bulb"
meat off grill	category	2	5.0	"take the — off the grill"
slide block	color	4	4.7	"slide the block to — target"
put in drawer	placement	3	12.0	"put the item in the — drawer"
push buttons	color	50	3.8	"push the — button, [then the — button]"
stack blocks	color, count	60	14.6	"stack — — blocks"
insert peg	color	20	5.0	"put the ring on the — spoke"
stack cups	color	20	10.0	"stack the other cups on top of the — cup"
place cups	count	3	11.5	"place — cups on the cup holder"
place wine	count	3	5.0	"stack the wine bottle to the — of the rack"

goals in the instructions are also modified while maintaining their semantic meaning. A summary of the 12 tasks is provided in Table 4.

We provide a detailed description of each task below and explain modifications from RLBench origin codebase.

B.1.1 Close Jar

Task: Close the jar by placing the lid on the jar.
filename: close_jar.py
Modified: The modified success condition registers a single DetectedCondition to check if the jar lid is correctly placed on the jar using a proximity sensor, discarding the previous condition of checking if nothing is grasped by the gripper.
Success Metric: The jar lid is successfully placed on the jar as detected by the proximity sensor.

B.1.2 Open Drawer

Task: Open the drawer by gripping the handle and pulling it open.
filename: open_drawer.py
Modified: The `cam_over_shoulder_left` camera's position and orientation were modified to better observe the drawer. The camera was repositioned to [0.2, 0.90, 1.10] and reoriented to [0.5*math.pi, 0, 0].

Success Metric: The drawer is successfully opened to the desired position as detected by the joint condition on the drawer's joint.

B.1.3 SCREW BULB

Task: Screw in the light bulb by picking it up from the holder and placing it into the lamp.
filename: light_bulb_in.py
Modified: No.
Success Metric: The light bulb is successfully screwed into the lamp and detected by the proximity sensor.

B.1.4 MEAT OFF GRILL

Task: Take the specified meat off the grill and place it next to the grill.
filename: meat_off_grill.py
Modified: The `cam_over_shoulder_right` camera's position and orientation were modified to better observe the drawer. The camera was repositioned to [0.20,-0.36,1.85] and reoriented to [-0.85*math.pi, 0, math.pi].
Success Metric: The specified meat is successfully removed from the grill and detected by the proximity sensor.

B.1.5 SLIDE BLOCK

Task: Slide the block to the target of a specified color.
filename: slide_block_to_color_target.py
Modified: No.
Success Metric: The block is successfully detected on top of the target color as indicated by the proximity sensor.

B.1.6 PUT IN DRAWER

Task: Put the item in the specified drawer.
filename: put_item_in_drawer.py
Modified: The `cam_over_shoulder_left` camera's position and orientation were modified to better observe the drawer. The camera was repositioned to [0.2, 0.90, 1.15] and reoriented to [0.5*math.pi, 0, 0].
Success Metric: The item is successfully placed in the drawer as detected by the proximity sensor.

B.1.7 PUSH BUTTONS

Task: Press the buttons of the specified color in order
filename: push_buttons.py
Modified: No.
Success Metric: The buttons are successfully pushed in order.

B.1.8 STACK BLOCKS

Task: Stack a specified number of blocks of the same color in a vertical stack.
filename: stack_blocks.py
Modified: No.
Success Metric: The blocks are successfully stacked according to the specified color and number.

B.1.9 INSERT PEG

Task: Insert a square ring onto the spoke with the specified color.
filename: insert_onto_square_peg.py
Modified: No.
Success Metric: The square ring is successfully placed onto the correctly colored spoke.

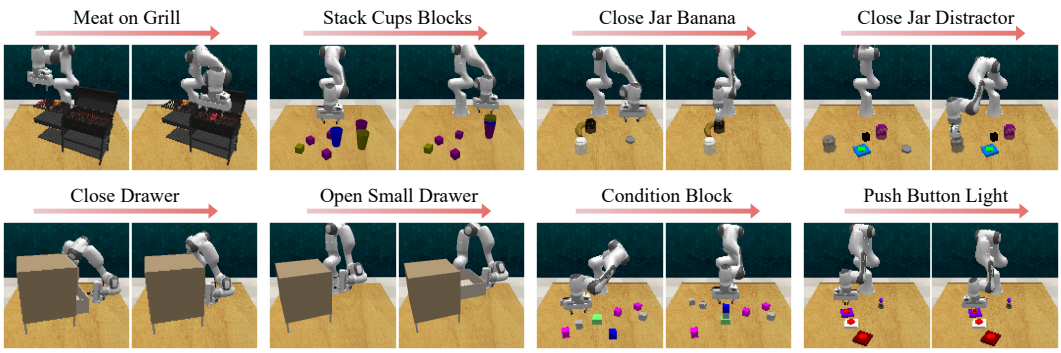

Figure 9: Visualization of 8 novel tasks.

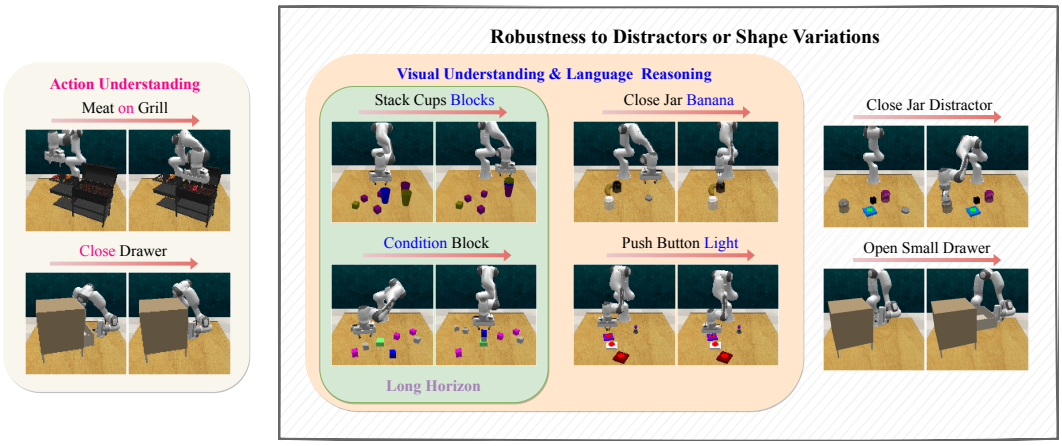

Figure 10: Three Novelty Categories for the Novel Tasks.

B.1.10 Stack Cups

Task: Stack two cups on top of the cup with the specified color.
filename: stack_cups.py
Modified: No.
Success Metric: The cups are successfully stacked with the correct cup as the base.

B.1.11 Place Cups

Task: Place a specified number of cups onto a cup holder.
filename: place_cups.py
Modified: No.
Success Metric: The cups are successfully placed onto the holder according to the task instructions.

B.1.12 Place Wine at Rack Location

Task: Place the wine bottle onto the specified location on the wine rack.
filename: place_wine_at_rack_location.py
Modified: No.
Success Metric: The wine bottle is successfully placed at the correct rack location and released from the gripper.

B.2 Novel Task

As shown in Fig. 9, we create 8 novel tasks that differ from the original training tasks to test policy generalization. These tasks feature scenes and objects similar to those in the training tasks. We

Table 5: The 8 novel tasks changed based on base tasks.

Task	Variation Type	# of Variations	Avg. Keyposes	Language Template
close drawer	placement	3	2.0	"close the — drawer"
close jar banana	placement	2	6.0	"close the jar closer to the banana"
close jar distractors	color	20	6.0	"close the — jar"
condition block	color, count	72	11.0	"build a tall tower out of — — cubes, and add a blue block if it exists"
meat on grill	category	2	5.0	"put the — on the grill"
open small drawer	placement	3	3.0	"open the — drawer"
stack cups blocks	color	20	10.0	"Identify the most common color in the block pile, and stack the other cups on the cup that matches that color"
push button light	color	20	2.0	"push the button with the same color as the light"

further define the novelty categories of the 8 novel tasks in our experiments to better explain the generalization improvements brought by GravMAD. As shown in Fig. 10, the designed novel tasks introduce three types of challenges to the model: **Action Understanding** (*meat on grill, close drawer*), **Visual Understanding & Language Reasoning** (*stack cups blocks, push buttons light, close jar banana, condition block*)—including two long-horizon tasks (*stack cups blocks* and *condition block*), and **Robustness to Distractors or Shape Variations** (*stack cups blocks, push buttons light, close jar banana, close jar distractor, open small drawer, condition block*).

Specifically, **Action Understanding** refers to tasks involving changes in interaction actions with objects; **Visual Understanding & Language Reasoning** involve introducing entirely new operational rules or conditions compared to known tasks; and **Robustness to Distractors or Shape Variations** includes tasks that require interaction based on fixed object attributes (such as color, size, distance, or distractors). A summary of the seven tasks is provided in Table 5. We provide a detailed description of each novel task below and explain the modifications from the base tasks.

B.2.1 Meat on Grill

Task: Place either a chicken or a steak on the grill depending on the variation.
filename: meat_on_grill.py
Base task: meat off grill.
Modified: The task requires placing meat onto the grill, whereas the base task involves removing it. The `cam_over_shoulder_right` camera's position and orientation were modified to better observe the drawer. The camera was repositioned to [0.20,-0.36,1.85] and reoriented to [-0.85*math.pi, 0, math.pi].
Success Metric: The selected meat (chicken or steak) is successfully placed on the grill and released from the gripper.

B.2.2 Stack Cups Blocks

Task: Identify the most common color in the block pile, and stack the other cups on the cup that matches that color.
filename: stack_cups_blocks.py
Base task: Stack cups.
Modified: The task involves identifying the cup that matches the most common color among the distractor blocks, then stacking the other two cups on top. The base task is simply stacking the cups without considering block colors.
Success Metric: Success is measured when the correct cup is stacked with the other cups based on the color identification and all cups are within the target area defined by the proximity sensor.

B.2.3 Close Jar Banana

Task: Close the jar that is closer to the banana by screwing on its lid.
filename: close_jar_banana.py
Base task: close jar.
Modified: The task involves identifying the jar closer to the banana and screwing its lid on, while the base task only requires closing a jar without proximity consideration.
Success Metric: The lid is successfully placed on the jar closest to the banana, confirmed by the proximity sensor.

B.2.4 CLOSE JAR DISTRACTOR

Task: Close the jar by screwing on the lid, while distractor objects are present.
filename: close_jar_distractor.py
Base task: close jar.
Modified: The task includes distractor objects, such as a button and block, which are colored and placed near the jars. These objects have been encountered during training, adding complexity compared to the base task.
Success Metric: The jar lid is successfully placed on the target jar, confirmed by the proximity sensor.

B.2.5 CLOSE DRAWER

Task: Close one of the drawers (bottom, middle, or top) by sliding it shut.
filename: close_drawer.py
Base task: open drawer.
Modified: The task involves closing the drawer instead of opening it.
Success Metric: The selected drawer is closed successfully, confirmed by the joint position of the drawer.

B.2.6 OPEN DRAWER SMALL

Task: Open one of the smaller drawers (bottom, middle, or top) by sliding it open.
filename: open_drawer_small.py
Base task: open drawer.
Modified: The task involves opening a smaller drawer compared to the base task, with adjusted camera settings for better visibility.
Success Metric: The selected drawer is opened successfully, verified by the joint position of the drawer.

B.2.7 CONDITION BLOCK

Task: Stack a specified number of blocks and, if the blue block is present, add it to the stack.
filename: condition_block.py
Base task: stack blocks.
Modified: The task involves stacking a specified number of blocks, with an additional requirement to include the blue block if it is present.
Success Metric: The correct number of target blocks are stacked, and if the blue block is present, it is also correctly added to the stack.

B.2.8 PUSH BUTTON LIGHT

Task: Push the button that matches the color of a light bulb on the first attempt.
filename: push_buttons_light.py
Base task: push button.
Modified: The task involves pressing a single button that matches the color of a light bulb. The button must be pressed correctly on the first attempt; repeated attempts are not allowed.
Success Metric: The correct button matching the light bulb's color is pressed on the first attempt.

B.3 FAILURE CASES OF GRAVMAD

In this section, we analyze why GravMAD underperforms compared to the baseline model 3D Diffuser Actor on certain base tasks, particularly in the *"Place Wine"* task and drawer-related tasks.

As discussed in the main paper, GravMaps represent spatial relationships in 3D space, but this introduces a challenge: areas close to the sub-goal often share the same cost value, as seen in the value map on the right side of Fig. 11 (a). This uniform cost value can mislead the robot into assuming it should complete the sub-goal within that area. For tasks requiring precise actions, such as the *"Open Drawer"* task, GravMaps' coarse guidance may lead to suboptimal performance compared to 3D Diffuser Actor. In the left schematic of Fig. 11(a), the robot must grasp the center of a small

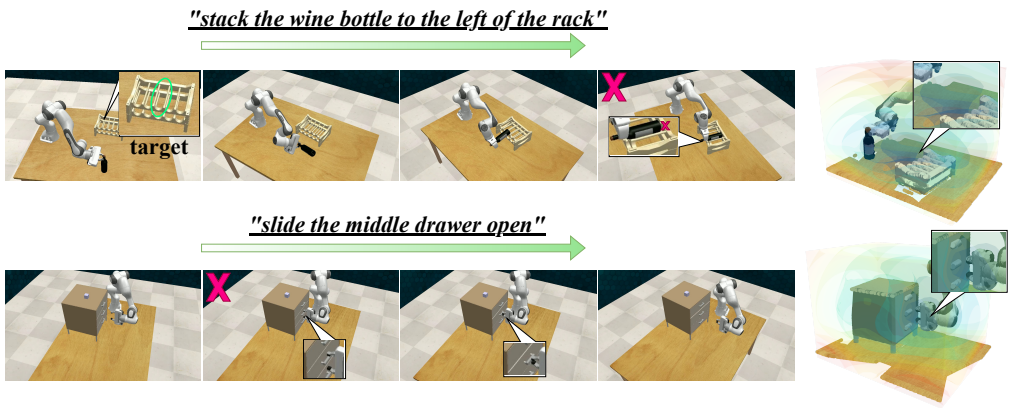

(a) Visualization of failure examples

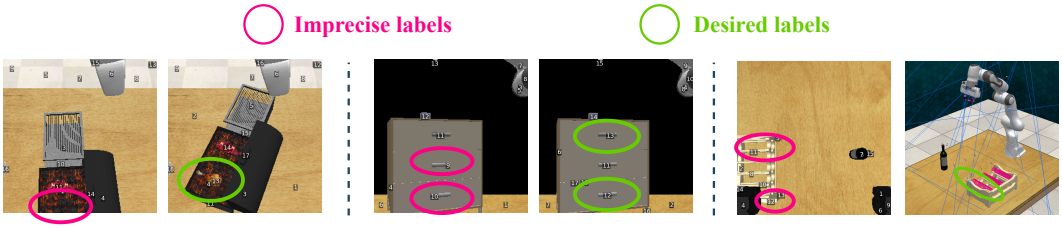

(b) Comparison of imprecise labels and desired labels

Figure 11: **Failure cause analysis**, including (a) visualization of failure examples; (b) comparison of imprecise labels and expected labels.

handle to achieve optimal performance in the *"Open Drawer"* task. This high precision demand on the end-effector results in a lower success rate for GravMAD. This limitation extends to the *"Put in Drawer"* task, which depends on the successful completion of *"Open Drawer"*. Similarly, in the *"Place Wine"* task, insufficient predictive accuracy causes the robot to misalign the bottle with the correct slot by one unit, leading to failure.

In the VLM setting, sub-goal accuracy often suffers, as shown in Fig. 11(b), further reducing model performance. These inaccuracies typically arise from two factors: (1) SAM may fail to accurately identify ideal areas, leading to imprecise contextual information from the Detector module for tasks like *"Place Wine"*, *"Open Drawer"*, and *"Put in Drawer"*; (2) the camera's positioning may not capture the full scene, leaving some task-relevant objects out of view, as seen in tasks like *"Meat off Grill"*. To overcome these VLM limitations, potential solutions include: (1) integrating multi-view information into the Detector for a more comprehensive scene observation; and (2) using a more granular segmentation model to provide GPT-4 with a wider range of labels, improving the quality of the context generated by the Detector.

C Discussion

C.1 The Relationship and Differences Between GravMap and Voxposer

The GravMap in GravMAD and the value maps in Voxposer (Huang et al., 2023) share the following connections and differences:

- **Number of value maps involved**: Voxposer utilizes multiple value maps, including the cost map, rotation map, gripper openness map, and velocity map. In our method, we only combine the cost map and gripper map, and their numerical values remain identical at this stage.

- **Structure and processing**: We further downsample the cost map and gripper openness map, transforming them into a point cloud structure containing position information and gripper states (x, y, z, m_c, m_g), which we term GravMap. This sparse data structure not only efficiently represents sub-goals but also allows feature extraction using a point cloud encoder.

C.2 The reason for not using the rotation map from Voxposer

GravMap does not currently use the rotation map from Voxposer because incorporating the rotation map could introduce significant distributional shifts between the guidance provided during the training and inference phases. During training, precise rotation guidance can be derived from expert trajectories. However, during inference, off-the-shelf foundation models often struggle to accurately interpret rotation information from visual and linguistic inputs, making it challenging to provide precise rotation guidance. To address this issue, future research will explore integrating rotation information from expert trajectories with object poses to generate few-shot prompts for off-the-shelf foundation models (Yin et al., 2024). This approach aims to enable LLMs to produce effective rotation guidance while reducing distributional shifts relative to the training data.

C.3 Further Details on Sub-goal Keypose Discovery

C.3.1 Why sub-goals are extracted differently during training and inference

During the training phase of GravMAD, we use Sub-goal Keypose Discovery to extract sub-goals and generate GravMaps based on them. In contrast, during the inference phase, sub-goals are inferred by foundation models to generate GravMaps. The reasons for adopting different methods to generate GravMaps during the training and inference phases are as follows:

- **Efficiency and reliability during training:** Using Sub-goal Keypose Discovery to extract sub-goals during training is both simple and efficient. If foundation models were directly used to generate GravMaps as guidance during training, while they can indeed produce GravMaps, the results are generally coarser, less precise, and slower compared to expert trajectories. For example, due to limitations such as camera resolution or angles, foundation models may fail to fully observe the scene in some cases, leading to inaccurate sub-goal positions (failure cases are discussed in Appendix B.3). Under such circumstances, the quality of the training data cannot be guaranteed. Additionally, using foundation models to process large-scale data is practically infeasible due to their slow processing speed.

- **Simplifying the problem by avoiding semantic reasoning:** Extracting sub-goals from expert trajectories focuses solely on analyzing the robot's actions, thereby avoiding the complexity of semantic understanding and reasoning. Our key insight is that in task trajectories, certain actions in expert trajectories inherently carry semantic information (i.e., sub-goals, which may involve direct interactions with objects). These actions often exhibit distinctive features, such as the opening and closing of the gripper. The Keypose Discovery method (James & Davison, 2022) has already performed an initial filtering of these key actions, narrowing the scope for sub-goal selection. Based on this, we can quickly identify sub-goals through heuristic methods, which are also effective for long-horizon tasks.

It is worth noting that using different sub-goal generation methods during the training and inference phases may lead to a distributional shift. This occurs because the sub-goals generated by foundation models during inference are often less precise compared to those derived from expert trajectories, resulting in a discrepancy between the distributions of the training and inference phases. To address this issue, we apply data augmentation to the precise sub-goals generated from expert trajectories during the training phase. Specifically, as described in Line 279 of Algorithm 1, we introduce random offsets to the sub-goals generated during training (this processing is not applied to sub-goals generated during inference) and then generate GravMaps based on these perturbed sub-goals. This approach effectively reduces the risk of distributional shift to a certain extent.

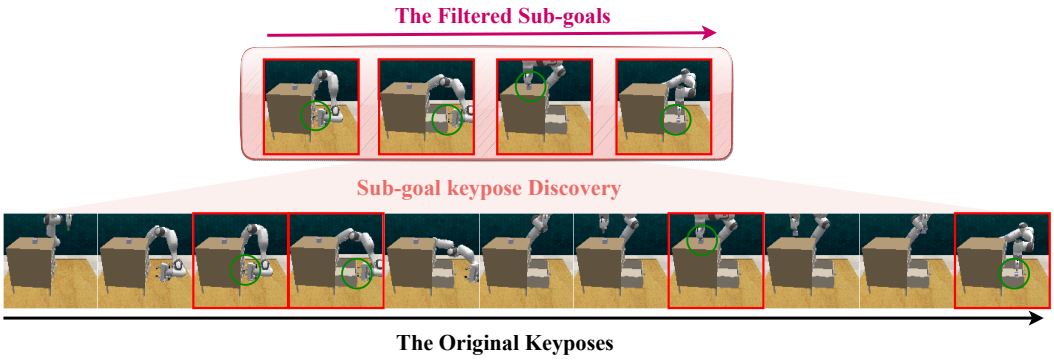

Figure 12: A comparison between the original keyposes and the filtered keyposes in the long-horizon task *put item in drawer*.

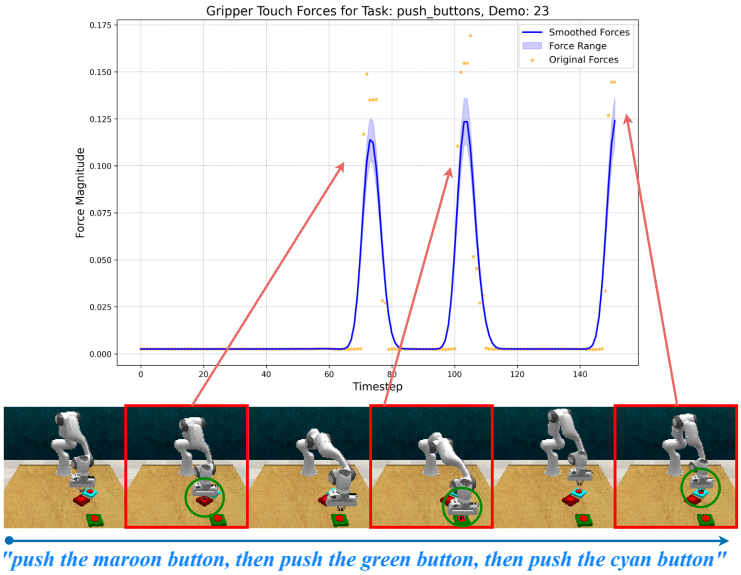

Figure 13: Visualization of sub-goal keypose discovery determining significant changes in **gripper_torch_force** during the *push button* task.

C.3.2 WHY USE SUB-GOAL KEYPOSE DISCOVERY TO FILTER KEYPOSES

The Sub-goal Keypose Discovery method is essential for GravMAD because the original keyposes include both sub-goal keyposes and the intermediate steps required to achieve these sub-goals. These intermediate steps may involve precise alignment of the robotic arm with objects. However, foundation models often struggle to generate these intermediate steps, and even if they can, the results may exhibit significant distributional shifts compared to the guidance provided during the training phase. Additionally, generating only sub-goals reduces the complexity and difficulty of task reasoning for the foundation model while also simplifying the prompt engineering.

As shown in Fig. 12, for the long-horizon task *put item in drawer*, if only traditional keypose discovery methods are used, the extracted sub-goal stages would include **11 stages**. In contrast, when using our Sub-goal Keypose Discovery, the filtered sub-goals are reduced to just **4 stages**, perfectly aligning with the most critical phases of the task. This significantly reduces model inference time and improves task execution efficiency.

	Voxposer	Act3D	3D Diffuser Actor	**GravMAD (ours)**
Avg. Inference Time for Keypose Prediction (secs)	/	0.04	1.78	1.81
Avg. Task Completion Time (secs)	448.01	14.08	49.45	97.04
Avg. Inference Time per Sub-task Stage (secs)	90.47	/	/	40.64

Table 6: Comparison of Inference Times.

Models	Avg. Success ↑	Avg. Rank ↓	Close Jar	Open Drawer	Meat off Grill	Slide Block	Put in Drawer
Voxposer	15.11	5.88	12.00	10.67	45.33	0.00	0.00
Voxposer (Manual)	22.06	4.92	13.33	18.67	69.33	0.00	0.00
ChainedDiffuser (Oracle)	29.72	4.42	82.67	0.00	52.00	2.67	0.00
Act3D	34.11	5.38	61.33	41.33	60.00	78.67	49.33
3D Diffuser Actor	55.81	3.00	66.67	88.00	88.00	84.00	94.67
GravMAD (Manual)	**69.17**	1.63	**100.00**	76.67	**89.33**	**93.33**	78.67
GravMAD (VLM)	56.72	2.79	**100.00**	58.67	70.67	80.00	61.33
Models	**Push Buttons**	**Stack Blocks**	**Place Cups**	**Place Wine**	**Screw Bulb**	**Insert Peg**	**Stack Cups**
Voxposer	80.00	16.00	6.67	5.33	4.00	0.00	1.33
Voxposer (Manual)	86.67	36.67	13.33	10.67	6.67	0.00	9.33
ChainedDiffuser (Oracle)	62.67	15.00	22.33	48.67	25.33	4.00	41.33
Act3D	66.67	0.00	0.00	45.33	6.67	0.00	0.00
3D Diffuser Actor	94.67	13.67	5.33	82.67	29.33	2.67	20.00
GravMAD (Manual)	**98.67**	**56.67**	5.33	77.33	**66.67**	**32.00**	**57.33**
GravMAD (VLM)	97.33	51.33	5.33	33.33	54.67	18.67	49.33

Table 7: Additional Multi-task test results on 12 base tasks.

Models	Avg. Success ↑	Avg. Rank ↓	Close Drawer	Close Jar Banana	Close Jar Distractor	Condition Block	Meat On Grill	Open Drawer Small	Stack cups blocks	Push Buttons Light
Voxposer (Huang et al., 2023)	34.29	3.25	96.00	17.33	22.67	25.00	38.67	6.67	0.00	68.00
ChainedDiffuser (Oracle) (Xian et al., 2023)	43.22	2.75	84.33	82.67	85.00	48.00	29.00	0.00	41.33	30.00
Act3D (Gervet et al., 2023)	17.83	4.25	66.67	29.33	41.33	0.00	1.33	2.67	0.00	1.33
3D Diffuser Actor (Ke et al., 2024)	29.38	3.375	81.33	48.00	42.67	27.00	0.00	2.67	2.67	30.67
GravMAD (VLM)	**62.92**	1.125	**97.33**	**84.00**	**86.67**	**74.00**	**45.33**	**21.33**	18.67	**76.00**

Table 8: Additional generalization results on 8 novel tasks.

C.3.3 Criteria for "Significant Changes" in Sub-goal Keypose Discovery

To clearly explain the specific criteria for "significant changes" in our Sub-goal Keypose Discovery method, we visualized the changes in **gripper_touch_force** using the *push buttons* task as an example. As shown in Fig. 13, when the button is pressed, the gripper_touch_force value increases from nearly 0 to 0.1 $\sim$ 0.15. As the robotic arm lifts, the gripper_touch_force returns to 0. By analyzing these force changes, we can intuitively identify the sub-goal frames.

D Additional Experimental Results

D.1 Inference Time

We test the inference time of all models under the setting of 8 novel tasks using a single NVIDIA 4090 GPU. The results, shown in Table 6 (in seconds), indicate the following: models like Act3D and 3D Diffuser Actor, which do not rely on foundation model inference, have shorter inference times but lower success rates. In contrast, Voxposer spends a significant amount of time synthesizing trajectories. Our GravMAD requires more time than Act3D and 3D Diffuser Actor because it waits for the foundation model to process information and infer sub-goals for sub-tasks.

D.2 Additional Baseline Experiments

We introduce two additional baseline methods for performance comparison: Voxposer (Manual) and Chained Diffuser (Xian et al., 2023) (Oracle). Voxposer (Manual) means that we manually provide ground truth object pose information to Voxposer instead of relying on the inference results of the foundation model. In Chained Diffuser (Oracle), we provide the ideal position for each keypose, with

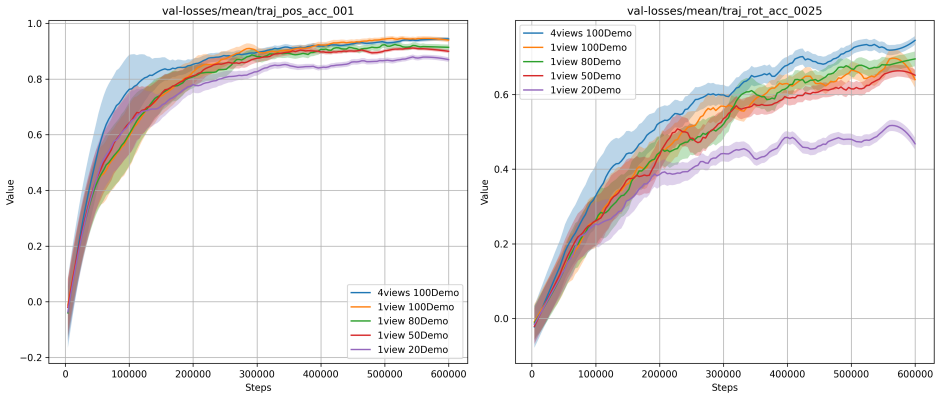

Figure 14: Comparison of validation curves under varying viewpoints and data sizes.

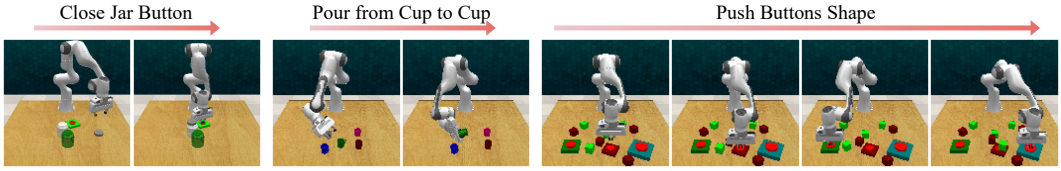

Figure 15: Visualization of additional novel tasks.

the connections between keyposes generated using the local trajectory diffuser module from Chained Diffuser. The performance comparisons of these two baseline methods on 12 base tasks and 8 novel tasks are shown in Table 7 and Table 8, respectively.

From the experimental results, we observe the following:

- In the base task setting, Voxposer (Manual) shows a slight performance improvement when provided with ground truth object information but still falls short compared to our GravMAD (Manual).
- For Chained Diffuser (Oracle), the keyposes come from ideal waypoints predefined in simulation, and the model effectively connects these keyposes, achieving a high success rate. However, in real-world scenarios, manually providing each keypose is impractical. Even with precise keyposes, Chained Diffuser (Oracle) still performs worse than our GravMAD (VLM).

D.3 Scalability of GravMAD

To evaluate the scalability of our proposed method with respect to data volume, we conduct training comparisons using five different demonstration dataset sizes and visualize the corresponding validation curves. The experimental results are presented in Fig. 14, with the validation curves reflecting two key metrics:

1) The proportion of predicted positions in the validation set with an error less than 0.01 (left subplot in Fig. 14).

2) The proportion of predicted rotations in the validation set with an error less than 0.025 (right subplot in Fig. 14).

The results in Fig. 14 clearly demonstrate that the model's performance improves as the number of expert demonstrations and the number of viewpoints increase. The key observations are as follows:

- With only 20 expert demonstrations, the model exhibits low overall performance, particularly in predicting rotation angles.

Task	Variation Type	# of Variations	Avg. Keyposes	Language Template
push button shape	color	20	2.0	"Press the buttons in order of their size, from smallest to largest"
button close jar	color	20	8.0	"after close the — jar, push the button"
pour from cup to cup	color	20	6.0	"pour liquid from the — cup to the — cup"

Table 9: Description of Additional Novel Tasks.

Additional Novel Task	**Voxposer**	**Act3D**	**3D Diffuser Actor**	**GravMAD (Ours)**
Push Buttons Shape (*Difficult Task*)	0	0	0	**62.66**
Button Close Jar (*Combination of Skills*)	0	0	0	0
Pour From Cup to Cup (*Completely New*)	0	0	0	0

Table 10: Generalization Performance Comparison on Additional Novel Tasks.

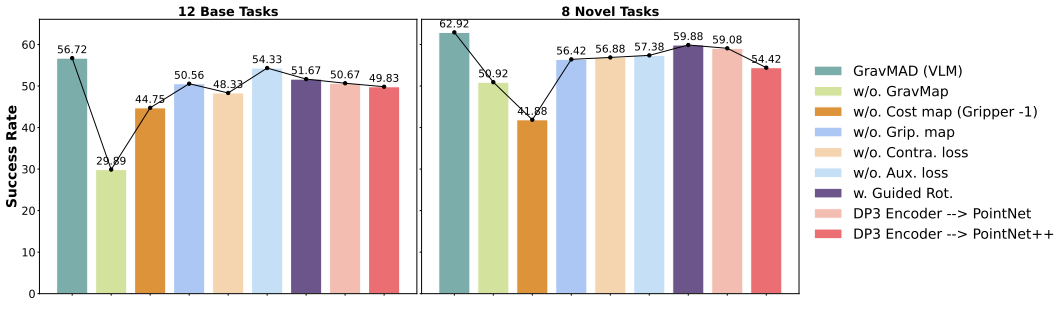

Figure 16: **Additional Ablation Studies**. We represent the gripper closure in the gripper map under "w/o. Cost map" as -1 instead of 0, enabling the encoder to correctly process this data structure.

- Models trained with four viewpoints achieve significantly better performance, but this improvement comes at the cost of increased training time.
- As the number of expert demonstrations grows, the marginal improvement in model performance diminishes. This could be attributed to the model's parameter size not scaling proportionally with the increase in data volume.

These results highlight the benefits of larger datasets for enhancing model performance. However, they also underscore the need for further optimization in model architecture and resource allocation to effectively harness the potential of large-scale data. Without such improvements, the diminishing returns observed with increasing data may limit scalability in practical applications.

D.4 Additional Novel Tasks

We evaluate the performance of baseline methods and GravMAD on three additional novel tasks, with detailed descriptions provided in Table 9 and Fig. 15. These tasks include a highly challenging one (Push Buttons Shape), a task that requires integrating skills learned during training (Button Close Jar), and a task involving entirely new objects compared to the training set (Pour From Cup to Cup).

The results are presented in Table 10 . The "Push Buttons Shape" task evaluates the model's ability to handle long-horizon planning, language reasoning, and robustness to visual perturbations. Under these conditions, all baseline methods fail to complete the task, whereas GravMAD performs well, showcasing its potential for generalization. For the "Button Close Jar" task, the results indicate that GravMAD still struggles with long-horizon tasks requiring the integration of multiple skills. In the entirely new task "Pour From Cup to Cup", GravMAD successfully identifies task-relevant objects but fails to complete the task due to incorrect actions. This failure is likely caused by a significant mismatch between the training data and the test environment.

D.5 Additional Ablation Study

To investigate the impact of the cost map on model performance, we perform more detailed experiments on the “w/o Cost map" ablation setting. In this ablation study, due to the inherent limitations of the encoder, the GravMap containing only the gripper map cannot be effectively processed. For instance, when the sub-goal requires the robotic arm to perform a “close everywhere" operation, m_g becomes a zero structure. Such an m_g cannot be properly parsed by the DP3 Encoder, resulting in gradient vanishing during the training process.

To address this issue, we modify the gripper map in the “w/o Cost map" setting by changing the closed state representation from 0 to -1, enabling the encoder to correctly process this data structure. The experimental results are shown in Fig. 16. The results show that removing the cost map causes a significant performance drop compared to the original model: a decrease of 11.97% on 12 base tasks and 21.04% on 8 novel tasks. These findings clearly highlight the critical role of the cost map in ensuring the performance of the GravMAD model.

D.6 Real World Evaluation

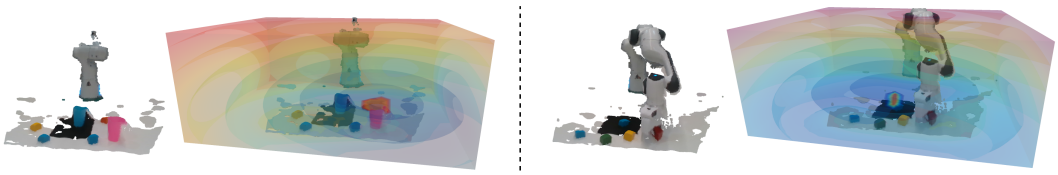

Real-world Task	Open Drawer	Toy in Drawer	Mouse on Pad	Stack Cup	Stack Block Same
GravMAD (%)	80	90	100	60	50
Real-world Task	**Place Cup**	**Stack Block**	**Stack Cup Blocks**	**Wired Mouse on Pad**	**Colored Toy in Drawer**
GravMAD (%)	10	40	40	100	70

Table 11: **Real-robot Results.** Success rates of GravMAD on 10 real-world tasks. These tasks include both manipulation and placement challenges. Above the table are the point clouds and GravMaps for Stack Cup Blocks and Stack Block, respectively.

We use a Franka Emika robot to validate GravMAD’s multi-task generalization ability across 10 real-world tasks. Each task involves variations in placement, and some tasks include color variations. Compared to the base tasks, the novel tasks introduce new objects and new instructions. The base tasks include:

- **Open Drawer** (task description: open top drawer)
- **Place Cup** (task description: put the yellow toy in the top drawer)
- **Mouse on Pad** (task description: put the wireless mouse on pad)
- **Stack Cup** (task description: stack color1 cup on top of color2 cup)
- **Stack Block Same** (task description: stack blocks with the same color)
- **Place Cup** (task description: place one cup on the cup holder)

The novel tasks involve:

- **Stack Block** (task description: stack color1 block on top of color2 block)
- **Stack Cup Blocks** (task description: identify the most common color in the block pile, and stack the other cups on the cup that matches that color)
- **Wired Mouse on Pad** (task description: put the wired mouse on pad)
- **Colored Toy in Drawer** (task description: put the Black and white toy in the top drawer)

We position a RealSense D435i camera in front of the robot to capture images, which are downsampled from the original resolution of 1280×720 to 256×256, as shown in fig. 17. During training, we collect 20 demonstrations for each base task to train the model. During inference, similar to the simulation setup, GravMAD predicts the next keypose, and we use the BiRRT planner provided by MoveIt! ROS to guide the robot to reach the predicted keypose. For evaluation, we run 10 episodes for each task and report the success rate.

The inference performance of GravMAD on 6 base tasks and 4 novel tasks is shown in Table 11. These results demonstrate that GravMAD can effectively reason about 3D manipulation tasks in real-world robotic scenarios, leveraging associated visual information and generalizing to novel tasks.

Figure 17: Real-Robot Setup with RealSense D435i and Franka Panda.

E Limitations and Potential Solutions

Despite GravMAD demonstrating strong generalization capabilities across the 3 categories and 8 novel tasks showcased, it still has certain limitations. The following section discusses some of the limitations not covered in the main text and their potential solutions:

- **Limitations of heuristic Sub-goal Keypose Discovery:** The current method relies on predefined heuristic rules, which may struggle to adapt to tasks with more complex or ambiguous sub-goal structures. Future research could explore more adaptive or learning-based strategies, such as incorporating diffusion models (Black et al., 2024) or generative models (Shridhar et al., 2024) to generate sub-goals, to further enhance the robustness and flexibility of the method.
- **Dependence on Detector accuracy and inference time:** The Detector's accuracy during the inference phase has a significant impact on the results, and its relatively long inference time remains a bottleneck. Future work could integrate observations from multiple viewpoints to provide a more comprehensive scene understanding and improve detection accuracy. Alternatively, more granular segmentation models could be leveraged to provide richer labels for foundation models, thereby improving the quality of the context generated by the Detector.
- **Limited guidance for end-effector orientation:** The current GravMap framework does not effectively guide the robot's end-effector orientation, limiting its applicability to tasks requiring precise orientation control. A potential improvement involves combining rotation information from expert trajectories with object poses to generate few-shot prompts for off-the-shelf foundation models (Yin et al., 2024). By leveraging such few-shot prompts, foundation models could produce more precise and effective rotation guidance.
- **Challenges in generalization:** While GravMAD performs exceptionally well on tasks similar to those seen during training, its generalization ability is still limited for tasks with significant differences from the training set, such as entirely unseen tasks or challenging tasks requiring a combination of multiple learned skills. Expanding GravMAD's capability to flexibly integrate multiple learned skills will be a key direction for future research.
- **Dependence on GravMap for Sub-goal Representation:** The GravMap framework relies on point cloud structures for sub-goal representation, which, while effective, may add unnecessary complexity in scenarios where simpler representations, such as a single point or relative coordinates, could suffice. The competitive performance of the "w/o GravMap" variant on novel tasks suggests that alternative representations could simplify the model without compromising performance. Defining sub-goals as relative coordinates with respect

to the gripper's current position, leveraging proprioceptive information, is a promising direction. This approach could possibly introduce more data variation, enhance adaptability to spatial changes, handle imprecise sub-goals, and naturally encode directional information. Future research could explore this direction further to achieve a balance between simplicity and performance, potentially enhancing the generalization capability of the model while reducing reliance on GravMap.

By addressing these limitations, we anticipate that GravMAD will demonstrate stronger adaptability and practical value in more diverse tasks.